JOURNAL OF GEOPHYSICAL RESEARCH, VOL. 103, NO. B3, PAGES 5037–5059, MARCH 10, 1998

A theory of intraplate tectonics

Shimon Wdowinski

Department of Geophysics and Planetary Sciences, Tel Aviv University, Ramat Aviv, Israel

Abstract. The theory of plate tectonics assumes a rigid behavior of tectonic plates and therefore fails to account for observed intraplate deformation. A new theory of intraplate tectonics is developed to calculate the first-order intraplate deformation induced by horizontal displacement of deformable plate boundaries. It is based on simple assumptions that link the well-established directions of relative plate motion to the displacement and deformation fields within a plate interior adjacent to three types of deformable plate boundaries: inward-, outward-, and tangential-displaced boundaries. The theory predicts the direction of intraplate displacement, displacement rate, strain, and stress fields in terms of small circles, great circles, and 45° loxodromes around the pole of rotation of two adjacent plates. The 45° loxodromes are two orthogonal sets of directions, clockwise and counterclockwise, that intersect both small and great circles at 45°. The principal axis of the maximum horizontal stress follows small circles for inward-displaced boundaries, great circles for outward-displaced boundaries, and loxodromes for tangential-displaced boundaries. The theoretical predictions are systematically compared with more than 4000 reliable observed directions of maximum horizontal stress provided by the world stress map project [*Zoback*, 1992]. The theory indicates that the first-order intraplate deformation is predominantly induced by horizontal forces acting on plate boundaries and by buoyancy forces that arise from lateral density variations between mid-ocean ridges and plate interiors (ridge push). The simplicity of the predictions and their good agreement with observations suggests that intraplate deformation should be investigated in the pole of rotation spherical coordinate system.

1. Introduction

The theory of plate tectonics has provided, for the past three decades, the geodynamic framework for the Earth sciences. Its fundamental postulate is that the Earth's outer shell, the lithosphere, is broken up into a finite number of rigid plates moving relative to one another [*Isacks et al.*, 1968; *Morgan*, 1968]. The rigid plate assumption allows us to predict the first-order kinematics of the Earth's surface in terms of relative or absolute plate motion; however, because no real material is absolutely rigid, this assumption also limits the theory's applicability. The theory can be successfully applied to plate interior regions, where intraplate deformation is negligible; in plate boundary regions characterized by significant intraplate deformation, however, the theory breaks down. The theory of plate tectonics is a poor approximation for the tectonics of many continental regions and some oceanic plate boundary regions [*Molnar*, 1988].

Paper number 97JB03390.
0148-0227/98/97JB-03390$09.00

Geophysicists have dealt with this issue by dividing the Earth's surface into two domains, nearly rigid plate interiors and deforming plate boundary regions, and treating deformation in each differently. Plate interiors, which show very limited permanent deformation, are generally treated as elastic plates deforming in response to tectonic and buoyancy forces [e.g., *Richardson et al.*, 1979; *Richardson and Reding*, 1991; *Richardson*, 1992; *Cloetingh and Wortel*, 1985, 1986; *Meijer and Wortel*, 1992; *Stefanick and Jurdy*, 1992; *Coblentz and Richardson*, 1996]. Plate boundary regions, where significant permanent deformation is usually observed, must be studied taking anelastic deformation into account. The kinematics of the deformation is commonly evaluated from the observed seismicity, which reflects most of the present-day permanent deformation [e.g., *Haines*, 1982; *Haines and Holt*, 1993; *Jackson and McKenzie*, 1984, 1988; *Ekstrom and England*, 1989]. Long-term deformation in plate boundary regions is commonly investigated by neglecting the elastic strength of the lithosphere and focusing on the cumulative permanent deformation by using plastic flow models [e.g., *Tapponier and Molnar*, 1976], viscous flow models [e.g., *England and McKenzie*, 1982; *Vilotte et al.*, 1982; *Bird and Baumgardner*, 1984], and viscoplastic flow models [e.g., *Wdowinski and Bock*,

1994]. In contrast, the elastic strength of the lithosphere plays an important role in studying short-term deformation, which is often described by the four stages of the earthquake deformation cycle: preseismic, coseismic, postseismic, and interseismic stages. Permanent deformation occurring during an earthquake (the coseismic stage) is usually described using elastic dislocation models [e.g., *Chinnery*, 1961, 1963]. Elastic strain accumulates steadily during the interseismic stage and is often investigated using locked fault models [*Savage*, 1983, 1990], elastic half-space block models [*Matsu'ura et al.*, 1986], and viscoelastic models [e.g., *Li and Rice*, 1987]; all three models assume that the upper crust behaves as a continuous elastic plate deforming in response to permanent deformation at depth, either due to slip on deep segments of faults or to viscous flow of the lower crust. Postseismic and preseismic deformation, which contribute only negligibly to the total deformation, are usually studied by models similar to those used for the interseismic deformation.

Studies of deformation in plate interior and plate boundary regions also differ in scale. Elastic deformation within plate interiors is usually studied at a plate or a regional scale [e.g., *Richardson*, 1992; *Coblentz and Richardson*, 1996]. In plate boundary regions, long-term permanent deformation is usually studied at a regional scale [e.g., *England and McKenzie*, 1982; *Vilotte et al.*, 1982] and short-term deformation at a local scale, which is defined according to the length of active fault segments [e.g., *Li and Rice*, 1987; *Bennett et al.*, 1996].

Because of the different ways that plate interiors and plate boundaries are modeled, all studies to date have focused on either one region or the other. In this study I develop a general framework for calculating regional scale elastic deformation in both regions. The deformation is analyzed following *Richardson*'s [1992] stress analysis, which considers two governing forces: horizontal forces acting on plate side boundaries and buoyancy forces that arise from lateral density variations between mid-ocean ridges and plate interiors (ridge push force). In plate interior regions, the deformation analysis is straightforward, because the deformation does not vary significantly with time. In plate boundary regions, however, the elastic deformation varies with time, as the magnitude of the driving forces exerted by the neighboring plate increases due to the steady motion of plates. The time dependency of the elastic deformation is obtained by calculating the displacement field at two or more time points and evaluating the rate of displacement change during a finite time span. Both types of analyses are synthesized into a new theory of intraplate tectonics that calculates the first-order intraplate displacement, strain, and stress fields in both plate interior and plate boundary regions. The theory yields testable predictions of the directions of the horizontal principal stress axes, which are successfully compared with more than 4000 reliable observations from the world stress project [*Zoback*, 1992]. Furthermore, comparing the observed and predicted directions of the horizontal stress field provides an additional independent quantitative estimate of the width of plate boundary regions that can be compared with estimates derived from seismic and geodetic observations. Although the theory focuses on elastic strain accumulation during the interseismic stage, it provides the first-order intraplate stress field, which determines the yield conditions at which permanent deformation (earthquake) occurs. The theory also provides a general reference frame for investigating intraplate displacement rate fields, which are observed nowadays by space geodetic techniques.

2. Intraplate Deformation

The present-day intraplate deformation can be evaluated from a variety of geophysical observations, including seismicity, strain and tilt meter measurements, in situ stress, and repeated geodetic measurements. Globally, the distribution of intraplate deformation can be evaluated from comprehensive data sets, which currently consist of two sets: global seismicity (Figure 1) and the world stress map [*Zoback*, 1992] (Figure 2). The regional distribution of present-day deformation can also be evaluated from various geodetic studies that measure changes in site positioning and distance changes between sites with time.

The global distribution of shallow earthquakes (depth 0-100 km, Figure 1) shows a high concentration of seismic activity in narrow belts along plate boundaries and minor activity within the interior of most plates. This well-known earthquake distribution led to the division of the Earth's solid surface into two major domains: (1) actively deforming plate boundary regions and (2) almost rigid plate interior regions. The width of the deforming plate boundary regions varies from a few hundred meters along some oceanic transform faults up to thousands of kilometers across diffuse plate boundaries, such as that between India and Eurasia [*Gordon*, 1995].

The world stress map (Figure 2) is a recent compilation of more than 4000 reliable stress orientation observations that shows the direction of maximum horizontal stress (SHmax) for various locations around the world [*Zoback et al.*, 1989; *Zoback*, 1992]. This data set shows distinct patterns that were evaluated visually [e.g., *Zoback*, 1992] and statistically [*Coblentz and Richardson*, 1995; *Bird and Li*, 1996]. The most prominent pattern is an almost uniform compressional stress field that exists in broad regions within plate interiors (e.g., eastern North America and western Europe). The uniform stress orientations in these areas were correlated with both absolute and relative plate motions [*Sbar and Sykes*, 1973; *Yang and Aggarwal*, 1981; *Gough*, 1984; *Zoback*, 1992; *Zoback and Zoback*, 1980, 1981; *Zoback et al.*, 1989]. These correlations suggest that the forces driving and resisting plate motion are the primary sources of most of the observed first-order stress field [*Richardson*, 1992; *Zoback*,

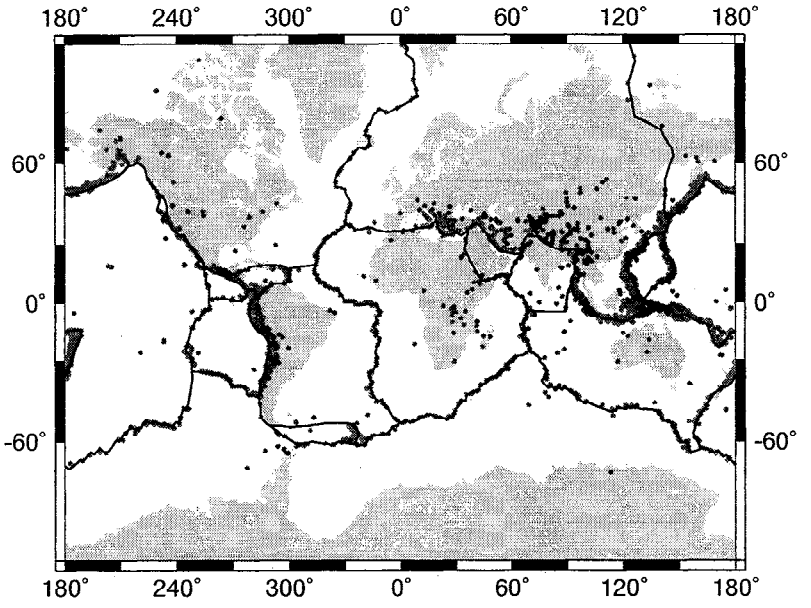

Figure 1. Global distribution of shallow (0-100 km) seismicity as listed in the Harvard centroid moment tensor catalog (1977-1994).

1992; *Zoback et al.*, 1989]. Orientation deviations from the first-order uniform stress field are attributed primarily to buoyancy forces related to crustal thickening and/or lithospheric thinning, but also to flexural stresses, smaller-scale lateral density contrasts, and lateral variations in crustal strength [*Zoback*, 1992]. Although the world stress map provides numerous observations from plate boundary regions, these observations have been largely ignored. A visual evaluation of stress orientations along plate boundaries, particularly along the Pacific Rim, shows a correlation between the orientation of SHmax and the direction of relative plate motion across these boundaries. This correlation is rigorously tested throughout this paper.

Recent advancements in space geodesy provide direct measurements of the intraplate displacement field within various plates. Geodetic measurements using Very Long Baseline Interferometry (VLBI), Satellite Laser Ranging (SLR), and Global Positioning System (GPS) have shown that the present-day displacement field in the stable parts of some of the major tectonic plates coincide with the predicted displacements determined by models of current plate motion (NUVEL-1A [*DeMets et al.*, 1994]), which are independent of

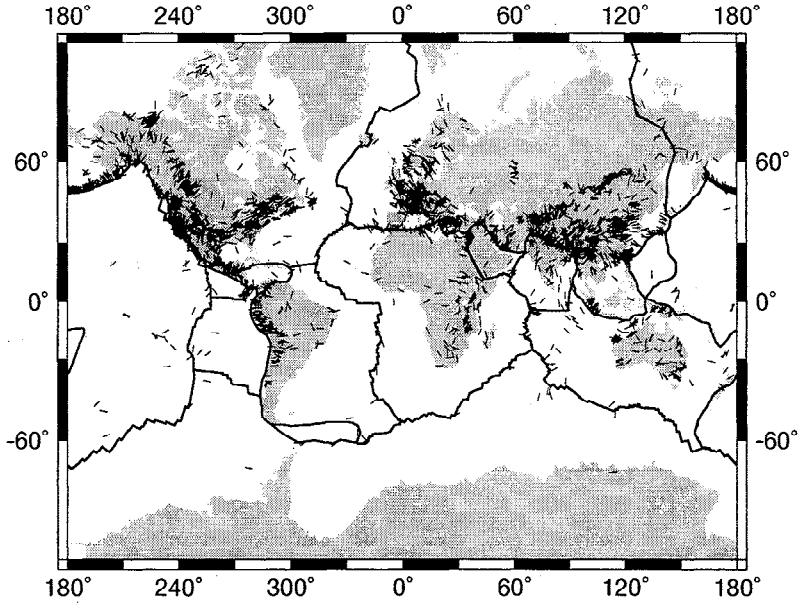

Figure 2. Global distribution of the direction of maximum horizontal stress as compiled by the world stress map project [*Zoback*, 1992].

geodetic measurements [*Herring et al.*, 1986; *Argus and Gordon*, 1990, 1996; *Ward*, 1988; *Smith et al.*, 1990; *Ray et al.*, 1991; *Ma et al.*, 1992; *Argus and Heflin*, 1995]. Measurements from tectonically active regions, however, indicate that the observed displacements diverge from those predicted by NUVEL-1A [e.g., *Ma et al.*, 1992; *Dixon*, 1993; *Feigl et al.*, 1993; *Tregoning et al.*, 1994; *Argus and Heflin*, 1995]. While in many regions the detected direction of the intraplate displacement rates are consistent with the velocity direction predicted by NUVEL-1A (e.g., southern California and many subduction zones), the detected magnitudes are significantly smaller than that expected from NUVEL-1A [e.g., *Dixon*, 1993; *Argus and Heflin*, 1995; *Bennett et al* 1996] (Figure 3). The reduced displacement rate is usually explained by elastic strain accumulation across a fault or an array of faults that is locked near the surface [e.g., *Savage*, 1983; *Matsu'ura et al.*, 1986].

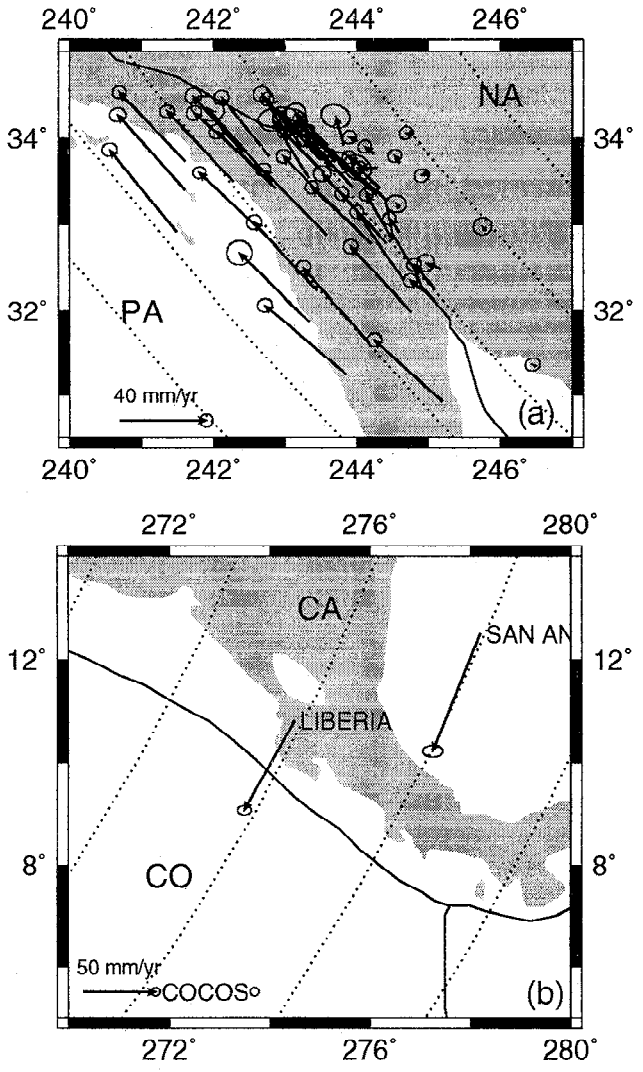

Figure 3. Regional distribution of the geodetically observed displacement rates (solid arrows) and the NUVEL-1A predicted relative plate motion (dotted lines) (a) in Baja and southern California in a fixed North America reference frame [after *Bennett et al.*, 1996] and (b) in Central America in a fixed Cocos plate reference frame [after *Dixon*, 1993].

The three sets of observations discussed above indicate three patterns of intraplate deformation: (1) plate interior regions are characterized by an almost uniform compressive stress field and negligible coseismic (earthquake) and interseismic deformation (below the sensitivity of current geodetic measurements), (2) plate boundary regions are characterized by significant coseismic and interseismic deformation, and (3) the displacement field and, in many cases, the stress field in plate boundary regions are parallel or subparallel to the direction of relative plate motion along the boundary.

3. Forces and Stresses

The forces that drive and resist plate motion were evaluated by *Forsyth and Uyeda* [1975]. Here I present a similar force analysis but with an emphasis on deformation within the plates. Tectonic plates, like all thin plates, deform in response to forces applied to their lateral boundaries, forces applied to the upper and lower surfaces of the plate, and to body forces. By constraining plate definition to fragments of the Earth's outermost strong shell (the lithosphere), subducting lithosphere is not considered part of a plate. However, forces induced by the subducting process (slab pull and slab drag forces [*Forsyth and Uyeda*, 1975]) can deform both overriding and subducting (outrise) plates and therefore are considered as forces that act on the base of plates.

Forces acting on plate side boundaries arise from the relative motion between two adjacent plates and thus are directed along the direction of relative plate motion. Along convergent plate boundaries, the forces are directed inward, toward the plate interior, and are often called collision resistance forces [*Forsyth and Uyeda*, 1975]. Along divergent plate boundaries the forces are directed outward, away from plate interiors. Along transform plate boundaries the forces are tangential to the boundaries and are often called transform resistance forces [*Forsyth and Uyeda*, 1975].

Forces acting on the upper surface of tectonic plates are exerted by the atmosphere and hydrosphere (oceans) and are negligible with respect to the other forces. Forces acting on the plate's lower boundary, which exert tractions on the base of the lithosphere, are induced by viscous shear between plates and the underlying mantle flow. Basal tractions due to viscous shear arise from differential motion between the plate and the underlying convecting mantle flow. As long as mantle flow and plates move in the same direction and at the same rate, no tractions act on the base of the plate. Small differential motion between the mantle and the overriding plate contributes insignificantly to intraplate deformation because of the low viscous coupling between mantle and plates. However, large differential motion, as occurs

near subduction zones, can generate significant basal tractions despite the relatively low viscosity of the mantle [*Wdowinski et al.*, 1989]. Additional sources of basal tractions above subduction zones are induced by slab pull and slab resisting forces; however, the two forces are poorly constrained and often are assumed to cancel each other. Overall, basal tractions contribute negligibly to intraplate deformation, except above subduction zones, where they have a limited localized effect.

Body forces acting on rock mass within the lithosphere give rise to intraplate deformation in regions characterized by significant lateral density variations. Topographic and density variations between mid-ocean ridge and subsided cold oceanic lithosphere results in a compressional deformation directed from the ridge inward toward the plate interior. The effect of this force is often viewed as an effective horizontal force acting on the ridge in the direction of relative plate motion - ridge push [*Forsyth and Uyeda*, 1975]. High elevated plateaus, such as Tibet or the Altiplano, are also a source for significant intraplate deformation resulting from lateral density variations. However, the deformation reflects mostly the shape of the plateau and is independent of plate velocities.

The forces acting on plates, which are in a dynamic equilibrium, cause the plates to be stressed. The orientation and magnitude of the stress field vary spatially, reflecting the distributions of the applied forces and spatial variations in the strength of the lithosphere. The stress field also varies temporally, as elastic strain accumulates during the interseismic stage and is released during earthquakes. The orientation of the intraplate stress field is evaluated from seismic data, in situ stress measurements, and the orientation of various structures. A large number of these measurements are presented by the world stress map (Figure 2) providing us a global distribution of the intraplate horizontal stress field. The magnitude of the intraplate stress field as estimated from seismic data is of the order of 100 MPa in plate interiors but possibly an order of magnitude less in plate boundary regions and in tectonically active zones within plates [*Ranalli*, 1987]. Stress magnitude changes occur in response to elastic strain accumulation between earthquakes and release during an earthquake (stress drop). Estimates for large earthquakes stress drop are in the range of 1-10 MPa [*Kanamori*, 1980]; although, laboratory experiments suggest that the stress drop is lower, ~1 MPa. Stress distribution calculations, which are based on elastic dislocation models, suggest a regional stress change in response to an earthquake. Because of the repeated occurrence of earthquakes along faults, the magnitude of the stress field adjacent to major faults varies with time and is often viewed as having a cyclic or a sawtooth pattern. The magnitude of stress field in regions located significantly far from fault zones (> 200 km) does not vary significantly during the timescale of the earthquake deformation cycle.

4. Theory

The force analysis and the observed intraplate deformation patterns are synthesized into a new theory of intraplate tectonics, which expands upon the classical theory of plate tectonics. Like the theory of plate tectonics, the new theory uses spherical geometry. The new theory is based on simple assumptions that link the well-established directions of relative plate motion to the displacement and deformation fields within plate interiors and plate boundary regions. It yields simple predictions about the direction of the intraplate displacement, strain, and stress fields, which are tested against the stress data of the stress map project.

4.1. Assumptions and Approximations

4.1.1. Tectonic plates are fragments of a thin spherical elastic-plastic shell. At the timescale of the earthquake deformation cycle, the lithosphere behaves elastically at low stress levels and plastically at stress levels that exceed the yield stress. Elastic (recoverable) deformation dominates the interseismic stage, whereas plastic (permanent) deformation dominates the coseismic stage. This study focuses on the elastic deformation of the interseismic stage.

Although elastic deformation is time-independent, elastic deformation in plate boundary regions varies with time and is evaluated in terms of displacement and strain rates. Temporal variations in the elastic strain field are caused by the continuous differential motion between plates exerting horizontal forces of increasing magnitude on plate side boundaries and by the release of accumulated elastic strain during earthquakes. At any given time, the forces can be evaluated and the time-independent elastic behavior of the lithosphere can be solved. An analogous example for this time varying elastic behavior during the interseismic stage is a slowly pushed or pulled spring, in which elastic deformation varies with time as the applied force increases or decreases.

4.1.2. Plates deform in response to (1) horizontal forces induced by their neighboring plates, and (2) buoyancy forces that arise from lateral density variations between mid-ocean ridges and plate interiors (ridge push). Horizontal forces acting on lateral plate boundaries are induced by their neighboring plates, as plates move relative to each other. The forces act on all side boundaries and are directed along the direction of relative plate motion between two adjacent plates. They induce boundary tractions according to the type of plate boundary (Figure 4). Along convergent boundaries (subduction zones and continental collision zones) the tractions are compressional; along divergent boundaries (spreading centers and continental rifts) the tractions are tensional; and, along transform and transcurrent boundaries, the two neighboring plates exert shear tractions tangential to

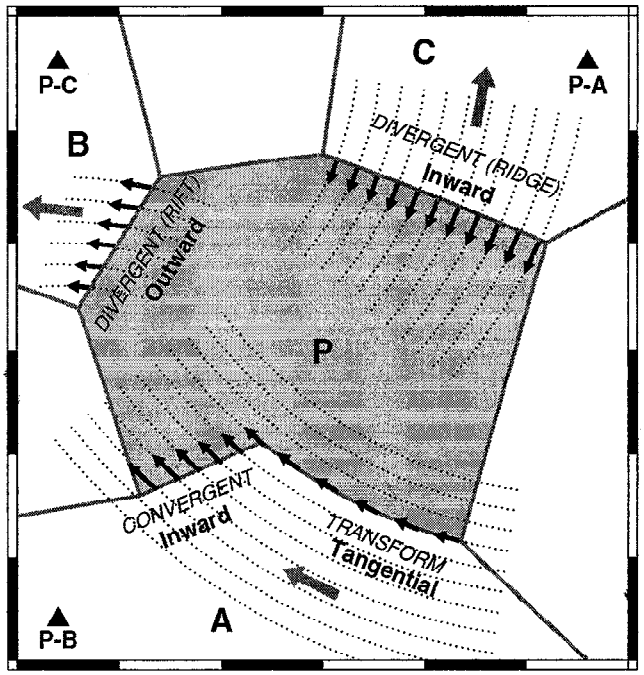

Figure 4. Schematic illustration of a deformable plate (P) with boundaries that are displaced inward, outward, and tangentially in the direction of relative plate motion (small circles, dotted lines) with respect to the adjacent plates. Poles of rotation are marked by solid triangles.

the orientation of the boundary. The tractions along an entire length of a plate boundary are assumed to have a uniform magnitude, representing a first-order average value. However, this value varies with time due to accumulation and release of elastic strain along the boundary fault zone. The traction magnitude is low immediately after a major earthquake and increases steadily with time as elastic strain is accumulated. Using a uniform traction condition and not uniform plate velocity condition is justified because the initiation and termination of the interseismic stage is controlled by the stress field and not by the displacement or velocity fields.

The theory also considers the effect of buoyancy forces that arise from lateral density variations between mid-ocean ridges and the plate interiors. The net effect of these forces is a compressional stress field that is directed from the ridge inward toward the plate interior. As in other studies [e.g., *Richardson*, 1992] these forces are applied as effective horizontal forces, ridge push, acting on plate side boundaries along ridges. The effective force induces compressional effective tractions directed inward, toward the plate interior. Because the lateral density variations between mid-ocean ridges and the plate interiors reflect the spreading and cooling history of the oceanic lithosphere, which is almost identical along the entire length of a ridge plate boundary, the effective tractions are assumed to have a uniform magnitude and to act perpendicular to the ridge, along the direction of relative motion. The very slow changes (million of years) in the density structure of oceanic plates suggest that the magnitude of the effective tractions is constant in the timescale of the earthquake deformation cycle.

The forces considered by the theory, which act on plate side boundaries, induce along each boundary a uniform traction field that is directed parallel to direction of relative plate motion. However, because the incremental displacement (displacement rate times a time span) field in plate boundary regions is better constrained than the stress field, it is more convenient to use boundary displacements rather than boundary tractions. By using linear elasticity, we can determine the direction and magnitude of the boundary displacement along each plate boundary. The boundary displacements also follow the direction of the relative plate motion between two adjacent plates (small circles, Figure 4). Their magnitude is highest at the Euler equator of relative plate motion and decreases with distance from the equator, reflecting the uniform traction condition in spherical coordinates.

The boundary displacement, which follows the direction of relative plate motion (small circles), define three types of deformable plate boundaries: inward-, outward- and tangential-displaced boundaries (Figure 4). Each boundary type describes the displacement of the boundary with respect to the plate interior. Inward-displaced boundaries lie along convergent (subduction and collision) rigid plate boundaries and along mid-ocean ridges. Outward-displaced boundaries lie along nonridge divergent boundaries (continental rifts), and tangential-displaced boundaries lie along transform plate boundaries. The difference between inward- and outward-displaced boundaries lies in the relative motion of the plate boundary toward or away from the plate interior. The boundary displacement is directed either toward or away from the plate interior and its magnitude varies with time along convergent boundaries and rifts, but is constant with time along mid-ocean ridges. Similarly, the boundary displacement of a tangential-displaced boundary is directed either clockwise or counterclockwise relative to the plate interior; its magnitude is also time-dependent.

4.1.3. Intraplate deformation concentrates in finite width regions parallel to one of the plate's boundaries. Variations in elastic strength and thickness within plates result in inhomogeneous deformation, in which weak regions of plates absorb most of the deformation. Tectonic plates can be divided into three major regions of similar strength: strong oceanic and stable continental regions, intermediate strength nonstable continental regions, and weak plate boundary regions. The deformation in entirely oceanic plates (e.g., Pacific or Nazca plates) and entirely continental plates (Arabian plate) is distributed throughout the entire width of the plate (Figures 5a, 5d, and 5g). Weak plate boundary regions, such as sections of plates overriding subduction zones mostly along the Pacific rim, absorb most of the deformation in a narrow region adjacent to the plate

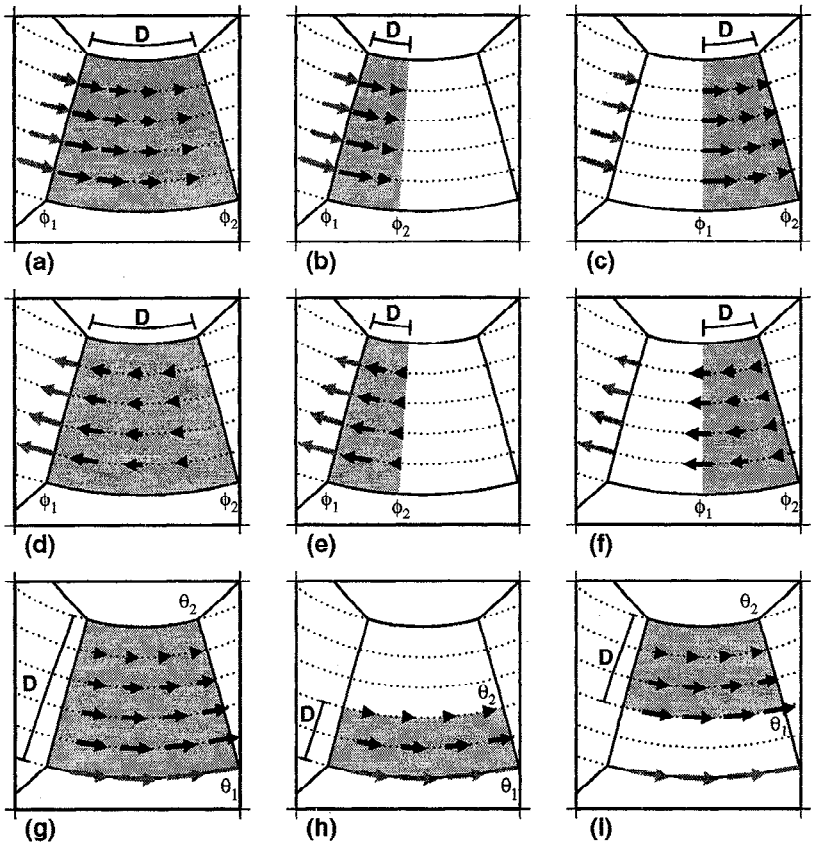

Figure 5. Schematic illustration showing the displacement field within three types of deformable plates, (left) homogeneous, (middle) weak plate boundary region, and (right) strong oceanic lithosphere, adjacent to the three type of plate boundaries (top) inward, (middle) outward, and (bottom) tangential. The deforming region (gray) is characterized by a finite width (D).

boundary (Figures 5b, 5e, and 5h). The deformation in combined oceanic-continental plates (e.g., North American, South American, Eurasian, African plates) concentrates in the weaker continental region of the plate; the strong oceanic region can be viewed as a rigid part of the plate that transmits the boundary tractions to the plate interior (Figures 5c, 5f, and 5i). Although the width of a deforming region varies along the length of a plate boundary, it is characterized by a single parameter (D, Figure 5), which represents a first-order average value.

4.1.4. Interseismic elastic deformation is homogeneously distributed within the deforming regions. During the interseismic stage of the earthquake deformation cycle, the deforming regions are subjected to (linear) elastic deformation, which is assumed to be homogeneously distributed throughout the width of the region. This assumption represents, once again, a first-order average strength value for each deforming region.

4.1.5. Thin Shell approximation (plane stress in spherical coordinates). This approximation is used to reduce the mathematical problem from three to two dimensions. It implies that the deformation within the shell occurs only in the colatitudinal and azimuthal components and is independent of the radial dimension. It can be used as long as (1) the shell's radial dimension is significantly smaller than the shell's colatitudinal and azimuthal dimensions and (2) all radial components of the stress tensor are negligible. The first condition is well justified, because the elastic thickness of the deforming regions is much smaller than the lateral dimension of these regions. Because the intraplate deformation is dominated by horizontal forces induced by the relative motion between plates and from lateral density variations between mid-ocean ridges and plate interiors (ridge push), it is reasonable to expect that the radial components of the stress tensor are negligible.

4.2. Formulation

The above assumptions allow us to formulate the theory in relatively simple expressions. As in the theory of plate tectonics, the tectonic plates are assumed to be fragments of a thin spherical shell, which are best treated using spherical geometry (Figure 6). The origin of the coordinate system is fixed at the Earth's center. However, the orientation of the pole changes for each plate boundary and is located at the pole of rotation describing the relative motion between the two neighboring plates. Because the radial component is equal

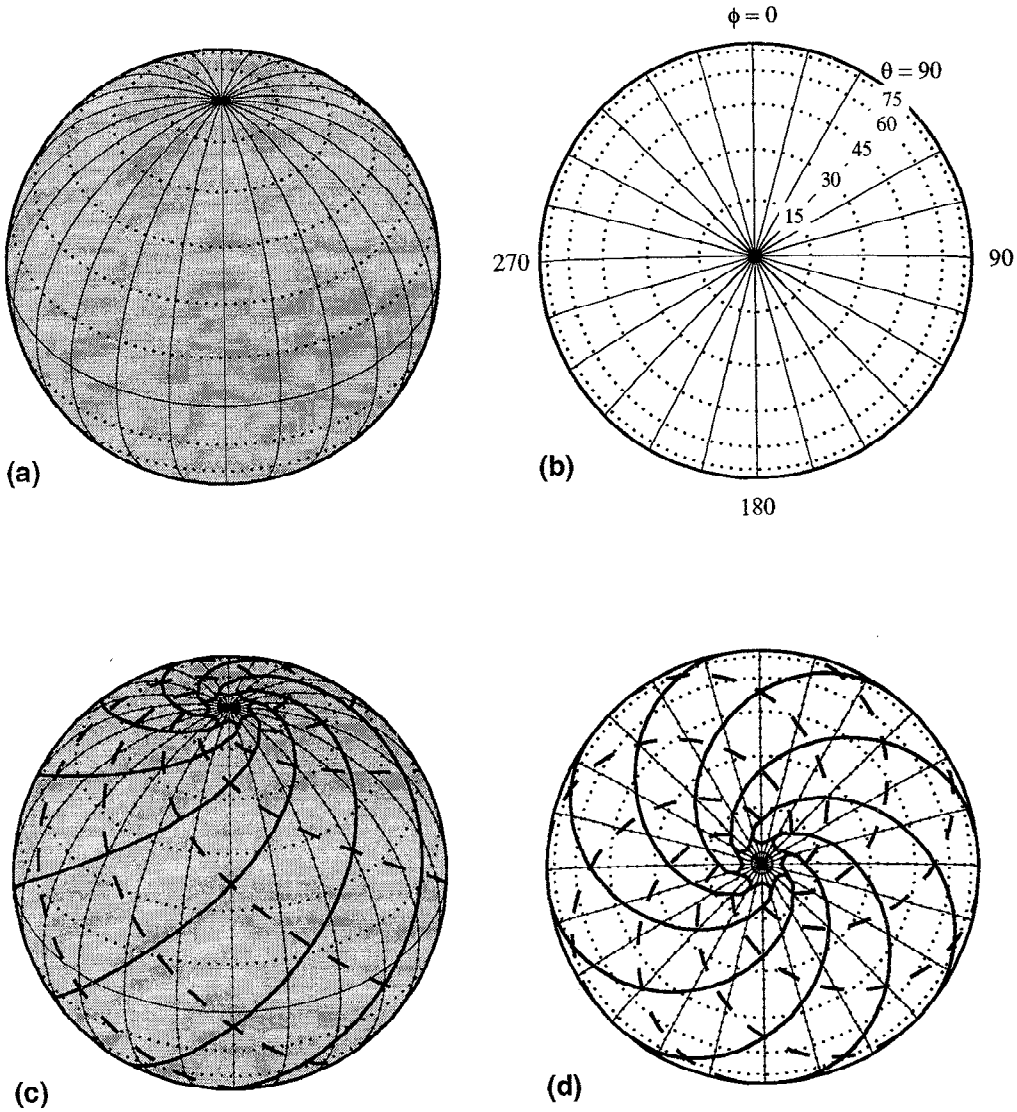

Figure 6. Spherical coordinate presentation of the Earth's surface as viewed (a, c) from an oblique angle to the pole of rotation (PoR) and (b, d) from directly above the PoR. Small circles are represented by thin dotted lines, great circles by thin solid lines, clockwise 45° loxodromes by thick solid lines, and counterclockwise 45° loxodromes by thick dashed lines.

everywhere on the sphere, the position of each point on the shell is determined by the colatitudinal and azimuthal coordinates (θ,ϕ). This coordinate system is represented by small and great circles; each small circle has a constant value of θ and each great circle has a constant value of ϕ (Figure 6).

The three nonradial components of the strain tensor [*Fung*, 1968, p. 113] are

$$\epsilon_{\theta\theta} = \frac{\partial u_\theta}{\partial \theta} \tag{1a}$$

$$\epsilon_{\phi\phi} = \frac{\partial u_\phi}{\partial \phi} + \sin^2\theta \cos^2\theta \, u_\theta \tag{1b}$$

$$\epsilon_{\theta\phi} = \frac{1}{2}\left(\frac{\partial u_\theta}{\partial \phi} + \frac{\partial u_\phi}{\partial \theta}\right) - \cot\theta \, u_\phi \tag{1c}$$

The colatitudinal and azimuthal angular displacements are

$$u_\theta = \frac{\xi_\theta}{r} \tag{2a}$$

$$u_\phi = \frac{\xi_\phi}{r \sin\theta} \tag{2b}$$

where ξ_θ and ξ_ϕ are the colatitudinal and azimuthal components of the displacement vector, and r is the sphere radius.

The plane stress approximation in spherical coordinates [*Wempner*, 1973, p. 465] yields the following equations

$$\sigma_{\theta\theta} = \frac{E}{1+\nu}\left(\epsilon_{\theta\theta} + \frac{\nu}{1-\nu}\,\epsilon_{\phi\phi}\right) \tag{3a}$$

$$\sigma_{\phi\phi} = \frac{E}{1+\nu}\left(\epsilon_{\phi\phi} + \frac{\nu}{(1-\nu)\sin^2\theta}\ \epsilon_{\theta\theta}\right) \quad (3b)$$

$$\sigma_{\theta\phi} = \frac{E}{1+\nu}\ \epsilon_{\theta\phi} \quad (3c)$$

where E is Young's modulus and ν is Poisson's ratio.

The above three equations provide the basic relations between the displacement, strain, and stress for a thin linear elastic shell. The equations are now applied to the three types of the deformable plate boundaries in order to calculate intraplate deformation adjacent to each boundary type. Because the kinematics of inward- and outward-displaced boundaries is very similar (differing from one another only in the direction of displacement), the mathematical treatment of both boundary types is identical. Similarly, the mathematical treatment of tangential-displaced boundary generates two solutions, one for a left-lateral tangential boundary displacement and the other for a right-lateral tangential boundary displacement. All solutions are time-independent and represent the elastic deformation at a given time. Using linear relations between boundary displacements and time (velocities), the time dependency of the interseismic deformation in plate boundary regions is also calculated.

4.3. Inward/Outward Displaced Boundaries

The displacement field adjacent to inward- and outward-displaced boundaries decays linearly along small circles, indicating a dependence only in the azimuthal direction (Figure 5). The linear decay results from the assumed linear elastic behavior of the deforming region. The two components of the intraplate displacement vector are

$$u_\theta = 0 \quad (4a)$$

$$u_\phi = u_0 \sin^2\theta\ \frac{\phi_2 - \phi}{\phi_2 - \phi_1} \quad (4b)$$

where u_0 is the magnitude of the boundary displacement at the Euler equator, and ϕ_1 and ϕ_2 are the bounding coordinates of the deforming region. Substituting (4) into (1) and (3) yields the following stress matrix

$$\sigma = -\frac{u_0 \sin^2\theta}{D}\ \frac{E}{1+\nu}\ \begin{pmatrix} \frac{\nu}{1-\nu} & 0 \\ 0 & 1 \end{pmatrix} \quad (5)$$

where D is the width of the deforming region ($D = \phi_2 - \phi_1$).

This stress field indicates that the principal axes of the stress tensor are oriented along small and great circles. For an inward-displaced boundary ($u_0 < 0$), the principal axis of maximum horizontal stress lies along small circles (Figure 7). In case of an outward-displaced boundary ($u_0 > 0$), the principal axis of maximum horizontal stress lies along great circles (Figure 7).

4.4. Tangential Displaced Boundaries

The displacement field adjacent to tangential-displaced boundaries decays linearly along great circles indicating a dependence only in the colatitudinal direction (Figure 5). The two components of the intraplate displacement vector are

$$u_\theta = 0 \quad (6a)$$

$$u_\phi = u_0 \sin^2\theta\ \frac{\theta_2 - \theta}{\theta_2 - \theta_1} \quad (6b)$$

and the derived stress matrix is

$$\sigma = -\frac{u_0 \sin^2\theta}{2D}\ \frac{E}{1+\nu}\ \begin{pmatrix} 0 & 1 \\ 1 & 0 \end{pmatrix} \quad (7)$$

where D is the width of the deforming region ($D = \theta_2 - \theta_1$).

This stress field indicates simple shear oriented along small circles, in which the principal axes of maximum and minimum stress are oriented at an angle of 45° to the direction of small and great circles. Geometrically, the principal axes follow 45° loxodromes that diverge clockwise and counterclockwise from the pole of rotation and intersect both small and great circles at angle of 45° (Figure 6). Loxodrome, also known as rhumb line, is a navigation term describing a line on a surface of a sphere, which make equal oblique angles with all meridians. A 45° loxodrome can be viewed as the path of an airplane flying from the north pole at an azimuth of 45° (counterclockwise loxodrome) or 135° (clockwise loxodrome). The 45° loxodromes are described by the following relations:

$$\phi = \phi_0 \pm \ln(\tan\theta/2) \quad (8)$$

where ϕ_0 is the rotation angle around the pole.

A right-lateral tangential displacement, which is represented by a positive value of u_0, yields a negative value of $\sigma_{\theta\phi}$ indicating that the principal axis of maximum stress is oriented along counterclockwise 45° loxodromes. Similarly, a left-lateral tangential displacement ($u_0 < 0$) yields a positive value of $\sigma_{\theta\phi}$, indicating that the principal axis of maximum stress is oriented along clockwise 45° loxodromes (Figure 7).

4.5. Time-Dependent Deformation

Temporal variations in interseismic deformation within plate boundary regions are caused by the continuous motion between plates, which exert horizontal forces of increasing magnitude on the plate lateral boundaries. As a result, the boundary displacements also increase with time; they are lowest immediately after a major earthquake and increase linearly with time. The time dependency of the deformation is introduced through the equatorial boundary displacement

$$u_0(t) = u_0(t_{eq}) + v_0 \times (t - t_{eq}) \quad (9)$$

Boundary	S_{Hmax} (solid lines)	S_{hmin} (dashed lines)	
Inward	Small circles	Great circles	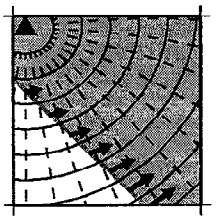
Outward	Great circles	Small circles	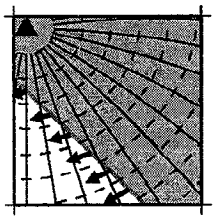
Tangential right-lateral	Counterclockwise loxodromes	Clockwise loxodromes	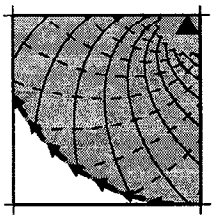
Tangential left-lateral	Clockwise loxodromes	Counterclockwise loxodromes	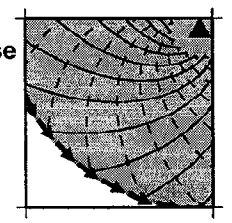

Figure 7. Predicted directions of maximum and minimum horizontal stresses adjacent to the various plate boundary types. Solid triangles show the location of poles of rotation.

where $u_0(t)$ is the equatorial boundary displacement at time t, $u_0(t_{eq})$ is the residual equatorial boundary displacement immediately after the last major earthquake, t_{eq} is the time at which the last earthquake occurred, and v_0 is the equatorial relative plate motion.

The time-dependent displacement field in plate boundary regions can be obtained by substituting (9) into (4) and (6), allowing us to calculate the intraplate displacement accumulated over a finite period of time. The displacement rates adjacent to inward- and outward-displaced boundaries are

$$\dot{u}_\theta = \frac{u_\theta(t_2) - u_\theta(t_1)}{t_2 - t_1} = 0 \qquad (10a)$$

$$\dot{u}_\phi = \frac{u_\phi(t_2) - u_\phi(t_1)}{t_2 - t_1} = v_0 \sin^2\theta \, \frac{\phi_2 - \phi}{\phi_2 - \phi_1} \qquad (10b)$$

and adjacent to tangential-displaced boundaries are

$$\dot{u}_\theta = \frac{u_\theta(t_2) - u_\theta(t_1)}{t_2 - t_1} = 0 \qquad (11a)$$

$$\dot{u}_\phi = \frac{u_\phi(t_2) - u_\phi(t_1)}{t_2 - t_1} = v_0 \sin^2\theta \, \frac{\theta_2 - \theta}{\theta_2 - \theta_1} \qquad (11b)$$

Both solutions show that the displacement rate field is oriented along small circles, parallel to the direction of relative plate motion. They also show that the displacement rate magnitude is related to the magnitude of the relative plate motion (v_0) and decays linearly from the plate boundary inward toward the plate interior. Adjacent to inward- and outward-displaced boundaries, the decay is along small circles, whereas adjacent to tangential-displaced boundaries the decay is along great circles.

The time-dependent intraplate stress field can be obtained by substituting (9) into (5) and (7). Adjacent to inward- and outward-displaced boundaries, the time-dependent stress is

$$\begin{aligned}\sigma(t) &= -[u_0(t_{eq}) + v_0 \times (t - t_{eq})] \\ &\times \frac{\sin^2\theta}{D} \frac{E}{1+\nu} \begin{pmatrix} \frac{\nu}{1-\nu} & 0 \\ 0 & 1 \end{pmatrix} \end{aligned} \quad (12)$$

and adjacent to tangential-displaced boundaries it is

$$\begin{aligned}\sigma(t) &= -[u_0(t_{eq}) + v_0 \times (t - t_{eq})] \\ &\times \frac{\sin^2\theta}{2D} \frac{E}{1+\nu} \begin{pmatrix} 0 & 1 \\ 1 & 0 \end{pmatrix} \end{aligned} \quad (13)$$

Both solutions show that the orientation of the stress field does not vary with time, but the stress magnitude increases steadily with time, as the two neighboring plates move with respect to each other.

4.6. Boundary Displacements

The above formulation provides simple geometrical relations for the orientation of the intraplate stress field adjacent to the three types of plate boundary (Figure 7). However, the stress field magnitude is poorly estimated by the equations, because it is related to the boundary displacement magnitude, which cannot be measured. Instead, I use the above expressions to estimate the magnitude of the boundary displacements. Independent estimates of the intraplate stress field [e.g., *Kanamori*, 1980] and of the ridge push force [e.g., *Richardson*, 1992] suggest that the magnitude of the intraplate stress field is in the range of 10-30 MPa, where the higher estimates reflect the stress field adjacent to ridge boundaries. Estimates for the lithospheric Young's modulus lie in the range of 30-70 GPa [e.g., *Turcotte and Schubert*, 1982]. Substituting the two estimates into (5) or (7) reveals that the boundary displacement, which also depends on the width of the deforming zone (D), is of the order of kilometers along ridge boundaries, and of the order of tens of meters along subduction and transform plate boundaries. Along the latter boundaries, however, the more important term is the incremental displacement, which is accumulated and released during the earthquake deformation cycle. The incremental displacement, as estimated from major earthquakes, lies in the range of a few meters, reflecting about 10% of the total displacement.

5. Testing the Theory

The theory predicts that the direction of the maximum horizontal stress (SHmax) follows, depending on the type of boundary, small circles, great circles, or 45° loxodromes around the pole of rotation (PoR) of the relative plate motion of two adjacent plates. In other words, the predicted orientation of SHmax with respect to the PoR is either 45°, 90°, 135°, or 180°. It also predicts that the intraplate stress field follows the predicted direction of SHmax in a finite width region. In this section I use the well-defined NUVEL-1A pole of rotations [*DeMets et al.*, 1994] to test the theory's predictions against more than 4000 reliable observations compiled by the world stress map [*Zoback*, 1992].

5.1. Methodology

A comparison between the observed and predicted directions of SHmax requires a coordinate transformation, because the observed data are described in the north pole coordinate system, and the theory's predictions are given in the PoR coordinate system. The simple geometrical relations of the predictions invite transformation of the observed data into the PoR system. Thus, in order to compare between the predictions and the observations, we need to calculate for each data point (1) the azimuth of SHmax with respect to the PoR and (2) the colatitudinal or azimuthal distance (in the PoR coordinate system) of the data point from a tested plate boundary.

The transformed azimuth is the angle difference between the observed azimuth of SHmax and the azimuth of a great circle in the PoR system that passes through the data point (Figures 8a and 8b). The mathematical description of this transformation is

$$\alpha_{QP} = \alpha_{obs} - \beta_{QP} \quad (14)$$

where α_{QP} is the transformed azimuth at a data point Q with respect to a pole P (PoR) and α_{obs} is the observed azimuth. The angle β_{QP} lies between two great circles that intersect at Q, where one passes through the north pole and the other passes through P.

$$\beta_{QP} = \cos^{-1}\left(\frac{\sin\theta_P - S\,\sin\theta_Q}{\sqrt{1-S^2}\,|\cos\theta_Q\,|}\right) \quad (15)$$

where S is

$$\begin{aligned} S &= \mathbf{P}\cdot\mathbf{Q} \quad (16)\\ S &= \cos\theta_P\cos\phi_P \times \cos\theta_Q\cos\phi_Q + \\ &\quad \cos\theta_P\sin\phi_P \times \cos\theta_Q\sin\phi_Q + \\ &\quad \sin\theta_P \times \sin\theta_Q \end{aligned}$$

and θ_P, θ_Q, ϕ_P, and ϕ_Q are the geographic colatitudes and longitudes of the points P and Q, respectively.

The colatitudinal or azimuthal distance of a data point from a tested plate boundary is the angle along small or great circles, respectively, that separates the data point from the boundary (Figures 8a and 8b). In order to obtain the distances in the PoR coordinate system, the geographic location of the data points and the boundary are transformed to the PoR coordinate system (Appendix). The calculation of the distances is conducted by a two-step procedure, which is (1) generation of a plate boundary table of positions in the PoR coordinate system $(\theta'_{PBj}, \phi'_{PBj})$ and (2) calculation of colatitudinal or azimuthal angle difference

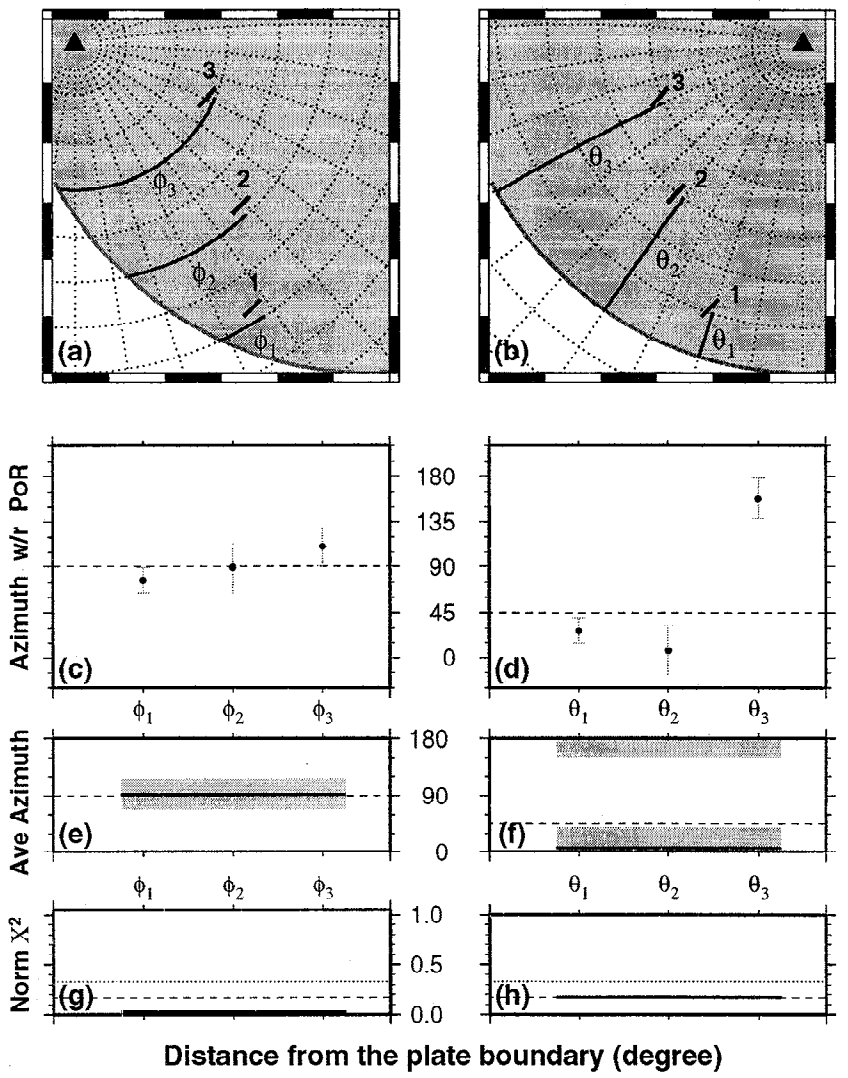

Figure 8. Schematic illustration showing the methodology used to test the theory. All six hypothetical data points in both maps (left inward/outward; right, tangential) are oriented at 45° with respect to the north pole but are located at various (a) azimuthal and (b) colatitudinal distances from the plate boundaries. (c, d) Same data points in the pole of rotation (PoR) coordinate system as a function of distance from the plate boundary. The dashed line indicates the expected orientation of the stress field by the theory. (e, f) Average azimuth (solid line) and the range of 1σ standard deviation (shaded area) of the data. (g, h) Results of the normalized χ^2 test. Dotted lines indicate the χ^2 of a randomly oriented data set and dashed lines indicate the cutoff for good fitting. The statistics of Figures 8f and 8h are operated on the range -45°-135°.

between each transformed data point (θ_i', ϕ_i') and the transformed plate boundary. For inward- or outward-displaced boundaries, the table of plate boundary positions is searched and interpolated according to the data point colatitude (θ_i') in order to find the azimuth of the plate boundary (ϕ'_{PB}). The azimuthal distance is

$$d\phi' = \phi'_{PB} - \phi'_i \tag{17}$$

For tangential-displaced boundaries the table of plate boundary positions is searched and interpolated according to the data point azimuth (ϕ_i') to find the colatitude of the plate boundary (θ'_{PB}). The colatitudinal distance is

$$d\theta' = \theta'_{PB} - \theta'_i \tag{18}$$

Figure 8 provides visual illustrations of the data transformation from the north pole coordinate system to the PoR coordinate system for both inward- and outward- and tangential-displaced boundaries. The hypothetical data points (Figures 8a and 8b), which are all oriented at an azimuth of 45°, are transformed to various orientations with respect to the PoR (Figures 8c and 8d). These points are also located along various distances from the plate boundary and are plotted accordingly in Figures 8c and 8d. The error bars represent hypothetical measurement errors, which are given in the data set of the world stress map project by the quality rank of

each data point [*Zoback*, 1992]. The transformed data can now be easily compared with the theoretically expected values of *SH*max (90°, 45°), shown as dashed lines in Figures 8c and 8d.

The observed and predicted direction of *SH*max are presented in two ways. The first presentation (Figures 8a and 8b) shows the observed direction in the standard way, in which the data points are oriented with respect to the north pole. The predicted directions of *SH*max are shown as dashed lines allowing a visual comparison between the two directions. The second presentation (Figures 8c and 8d) shows the observed direction of *SH*max in the PoR reference frame, in which the predicted directions are straight lines. This presentation, which also shows measurement uncertainties, allow a rigorous comparison between the observed and predicted directions, as a whole or with respect to the distance from the plate boundary. The disadvantage of the second presentation is that it does not indicate regions characterized by an anomalous stress field; however, the anomalous regions can be evaluated from the first presentation. The actual comparison between the observed and predicted directions of *SH*max is conducted statistically.

5.2. Statistical Tests

A quantitative comparison between the predicted and observed directions of *SH*max is obtained by the calculation of the average azimuth and by a normalized χ^2 test. The average azimuth (solid lines in Figures 8e and 8f) and its 1σ standard deviation range (shaded area in Figures 8e and 8f) are good indicators of the quality of the fit between the predicted and observed azimuths of *SH*max. Figure 8e presents an example of a very good fit, in which the average observed azimuth differs by 2° from the predicted azimuth and its standard deviation is 24°. Figure 8f presents an example of a very bad fit, in which the predicted azimuth differs by 40° from the average azimuth and lies beyond the range of 1σ standard deviation.

A more rigorous comparison between the predicted and observed directions of *SH*max is obtained by a normalized χ^2 test. This test uses the reported uncertainties of the observed azimuth (quality rank) to better evaluate the fit between the two azimuths. A regular χ^2 test is not indicative of the fit because the tested population varies from one plate boundary to another. Therefore results of the χ^2 test are normalized by the worst case scenario, which is 90° difference between the the predicted and observed azimuth. The normalized χ^2 test is

$$\text{Norm } \chi_j^2 = \frac{\sum_{i=1}^{M} \left(\frac{\alpha_i - \alpha_{\text{predict}}}{\sigma_i} \right)^2}{\sum_{i=1}^{M} \left(\frac{90}{\sigma_i} \right)^2} \qquad (19)$$

where α_i and α_{predict} are the observed and predicted directions of *SH*max with respect to the PoR, respectively. The σ_i parameter is the reported uncertainty of the observed azimuth and M is the number of observations that are used in each test.

The normalized χ^2 test yields a number in the range 0-1, which indicates the quality of the fit. Low values of Norm χ^2 ($\leq$ 0.15, dashed lines in Figures 8g and 8h). indicates good agreement between predicted and observed directions. High values of Norm χ^2 ($>$ 0.7) indicates a systematic misfit between predicted and observed directions of about 90°. Random distribution of *SH*max directions results in Norm χ^2 = 0.33 (dotted lines in Figures 8g and 8h). In the examples of Figure 8, the hypothetical data points yield both a very low (0.03 in Figure 8g) and a high (0.17 in Figure 8h) value of Norm χ^2. The very low value indicates a very good fit between the observed and predicted azimuths of *SH*max , whereas the high value indicates a bad fit between the two azimuths.

5.3. Results

I conducted a systematic comparison between the theory's predictions and the observed direction of *SH*max (Figure 2) along the 34 major plate boundaries. Table 1 summarizes the results of the most significant tests. The rest of the tests were inconclusive, principally because of a lack of sufficient stress observations. The observed azimuth (with respect to the PoR) in Table 1 represents the average azimuth of all the data points that lie between the lower and upper limits of the deforming region. For inward- or outward-displaced boundaries, the limits are the azimuthal coordinates (ϕ_1 and ϕ_2) of the deforming region boundaries in the PoR coordinate system, whereas for tangential-displaced boundaries, the limits are the colatitudinal coordinates (θ_1 and θ_2). The width (D) reflects the coordinate difference between the upper and lower limits of the deforming region. The limits are determined according to the lowest normalized χ^2 value of all possible ranges of limits (incremented by 1°-2° in plate boundary regions and by 5° in plate interior regions) that show significant statistical results.

Table 1 shows a very good agreement between the predicted and observed (average) directions of *SH*max . The statistical significance of these results is represented by both the 1σ standard deviation and the normalized χ^2. Regions with a good fit are represented by lower values of the standard deviation (18°-35°) and normalized χ^2 (0.03-0.15). The very low values of both properties in the Eurasia-Pacific plate boundary (Japan) are calculated from only four data points and therefore have very little significance. Higher values of the two statistical parameters indicate intermediate to bad fit between the predicted and observed directions of *SH*max . Based on the χ^2 criterion, Table 1 shows that the theory predicts well stress field in 17 of the listed 21 regions. The width of the deforming region varies from 4° to 8° in narrow plate boundary deformation regions, from 10° to 20° in

Table 1. Statistical Parameters and Test Results for Deforming Regions Adjacent to the Various Plate Boundaries

Boundary	Region	Type	Predicted Azimuth	Observed Azimuth	Norm χ^2	Data Points	Lower Limit ϕ_1 / θ_1	Upper Limit ϕ_2 / θ_2	Width D
				Americas					
na-pa	Aleutians	Inward	90	94 ± 30	0.11	259	0	4	4
na-pa	Queen Charlotte	Tan (R)	135	134 ± 18	0.03	107	-1	12	13
na-jf	Cascadia	Inward	90	72 ± 31	0.12	304	0	13	13
na-pa	Southern California	Tan (R)	135	144 ± 28	0.09	419	-3	8	11
na-co	Central America eastern	Inward	90	94 ± 43	0.18	91	0	35	35
na-eu	North America	Inward	90	89 ± 32	0.11	329	24	50	26
na-ca	northern Caribbean	Tan (L)	45	49 ± 31	0.09	40	-5	2	7
co-ca	Central America northern	Inward	90	88 ± 38	0.18	69	0	15	15
sa-ca	South America eastern	Inward	90	85 ± 39	0.18	42	0	8	8
sa-af	South America	Inward	90	76 ± 30	0.10	160	35	70	35
sa-nz	Andes	Inward	90	103 ± 20	0.07	109	0	6	6
				Eurasia					
eu-af	western Europe	Inward	90	98 ± 29	0.09	233	20	34	14
eu-ar	Iran	Inward	90	98 ± 27	0.10	40	2	12	10
eu-in	Tibet	Inward	90	91 ± 36	0.15	276	0	20	20
eu-au	Indonesia	Inward	90	105 ± 24	0.10	276	0	6	6
eu-ph	SE Asia	Inward	90	90 ± 33	0.12	35	0	3	3
eu-pa	Japan	Inward	90	91 ± 7	0.00	4	0	4	4
				Other Plates					
ar-af	Arabia	Inward	90	86 ± 46	0.25	12	0	6	6
in-eu	India	Inward	90	90 ± 34	0.13	26	10	40	30
nu-so	eastern Africa	Outward	180	184 ± 32	0.13	74	-10	10	20
au-af	eastern Africa	Outward	180	174 ± 31	0.10	121	-30	30	60

Plate abbreviations are af, Africa; an, Antartica; ar, Arabia; au, Australia; ca, Caribbean; co, Cocos; eu, Eurasia; in, India; jf, Juan de Fuca; na, North America; nu, Nubia; nz, Nazca; pa, Pacific; sa, South America; so, Somalia. Tangetial (Tan) plate boundaries are either right (R) or left (L) lateral. The azimuths, the coordinates of the lower and upper limits, and the width of the deforming region are in degrees.

plate boundary regions with diffuse deformation, and from 20° to 60° in plate interior regions.

In the rest of this section I elaborate on results of eight tests of the intraplate stress field adjacent to the three types of deformable plate boundaries: inward-, outward-, and tangential-displaced boundaries. In order to evaluate the agreement between predicted and observed azimuths as a function of distance from the plate boundary, the statistical tests are conducted on segments of the data. The first set of tests (Figure 9) show examples of inward- and tangential-displaced plate boundaries that lie along two segments of the Pacific-North America plate boundary. The second set (Figure 10) examines the stress field within the interiors of two plates, eastern North America and western Eurasia. The third set (Figure 11) examines the stress field in South America, viewing it as a plate boundary deformation along the South America-Nazca boundary or as plate interior deformation influenced by the ridge push along the South America-Africa boundary. The last set of tests (Figure 12) examines the extensional stress field within eastern Africa.

5.3.1. Western North America. Figure 9 shows the observed and predicted intraplate stress field adjacent to the Pacific-North America plate boundary along two segments: the Aleutian island arc (Figure 9a) and the San Andreas-Gulf of California segment (Figure 9b). The Aleutian arc represents a convergent plate boundary where the Pacific plate subducts underneath the North American plate. According to the theory, this is an inward-displaced boundary, in which direction of *SH*max should follow the orientation of small circles. This prediction is tested by transforming the observed direction of *SH*max into the PoR coordinate system (Figure 9c). The cluster of observations along the predicted azimuth of 90° and the two statistical tests (Fig-

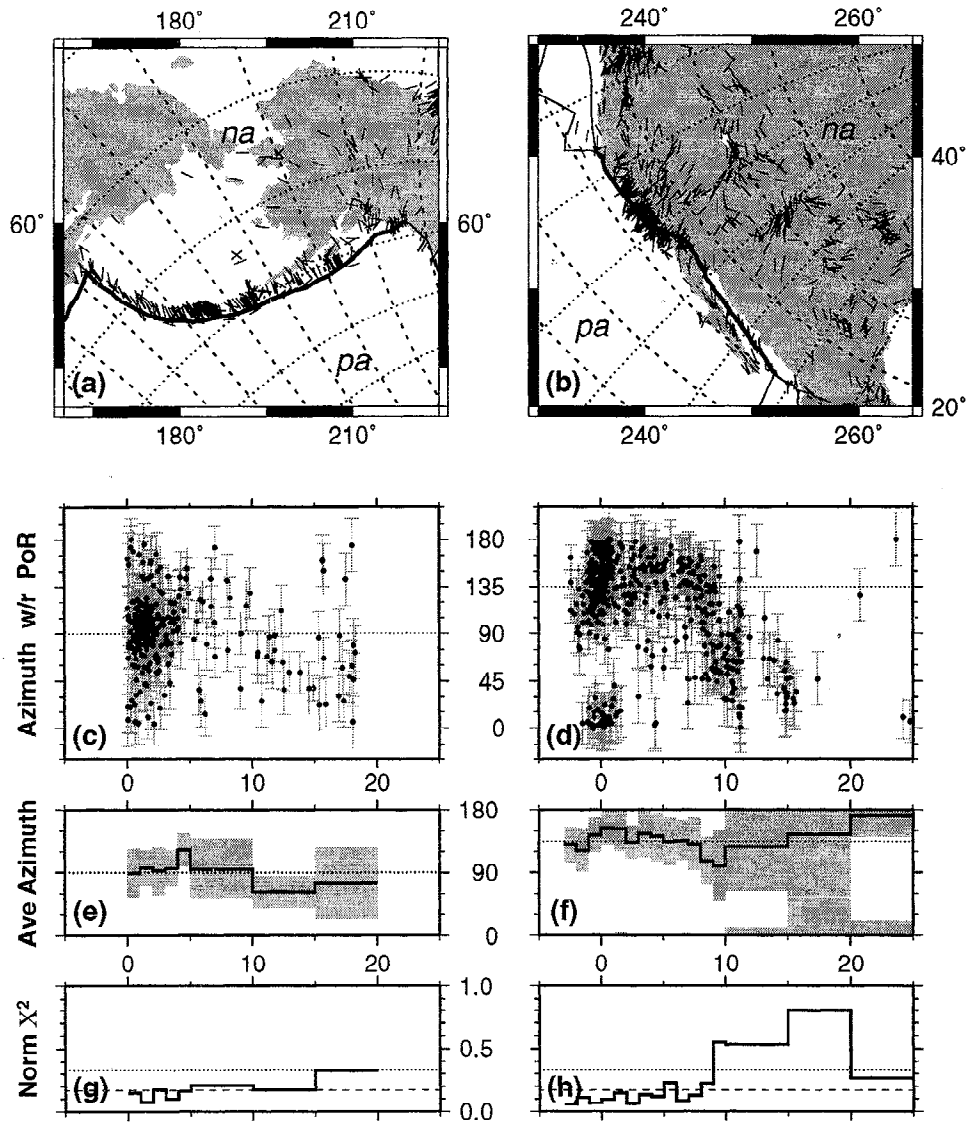

Figure 9. Intraplate stress field in North America adjacent to the Pacific plate boundary. The data along the Aleutian arc are consistent with the stress field predicted for an inward-displaced boundary and the data from the San Andreas-Gulf of California segment are consistent with the stress field predicted for a tangential-displaced boundary. (a, b) Maps of the region showing the orientation of *SH*max as compiled by the world stress map project. Dotted lines denote 10° great circles and short-dashed lines denote 5° small circles with respect to the North America-Pacific PoR. (c, d) The orientation of *SH*max and the reported standard deviation of the data in the PoR coordinate system. (e, f) Average azimuth of the data and its 1σ standard deviation (shaded area). (g, h) Results of the normalized χ^2 test. The statistics of Figures 9f and 9h are operated on the range 45°-225° .

ures 9e and 9g) indicate a good agreement between the predicted and observed azimuths in the distance of 0°-4° from the plate boundary. Farther away from the plate boundary the data are scattered at various azimuths.

The San Andreas-Gulf of California segment of the Pacific-North America plate boundary is a transform plate boundary that lies along a small circle (Figure 9b). According to the theory, this is a right-lateral tangential-displaced boundary, in which the direction of *SH*max should follow counterclockwise 45° loxodromes around the PoR. Indeed, the transformed data show a large concentration of observations around the 135° predicted azimuth of *SH*max (Figure 9d). The statistical tests show a good agreement between the observed and predicted values of *SH*max for the distance of -3°-8° from the plate boundary (Figures 9f and 9h). Although the stress field contiguous to the San Andreas fault is aligned perpendicular to the fault (180° with respect to

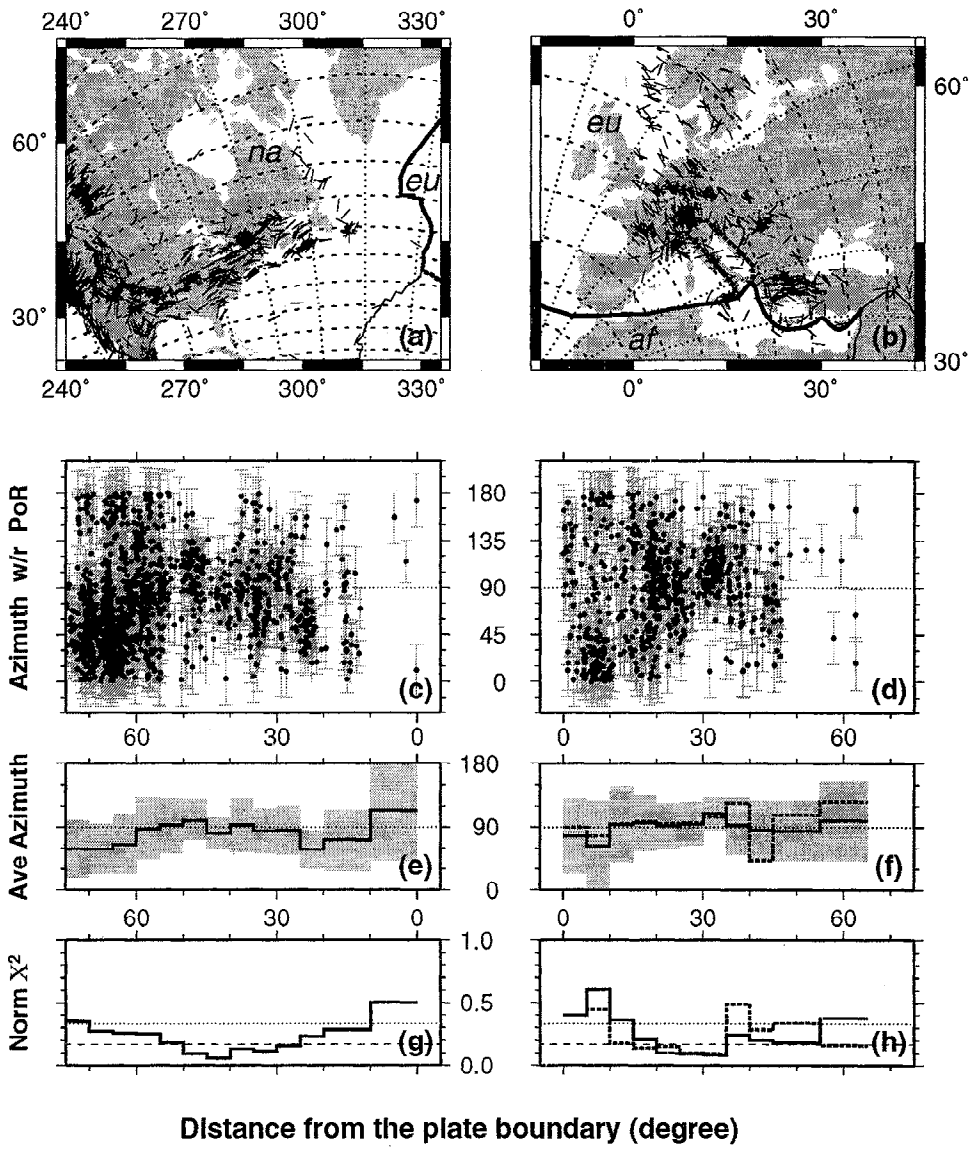

Figure 10. Intraplate stress field in (a) eastern North America and (b) western Europe. The data in the interior of both plates are consistent with the stress field predicted by an inward-displaced boundary. See Figure 9 for details. Dashed lines represent statistical tests that include the Adriatic Sea and exclude the Hellenic arc from the Eurasian-Africa plate boundary.

PoR), the statistical tests of the entire plate boundary show only a small increase in the average azimuth at a distance of -2°-2° from the boundary.

5.3.2. Eastern North America. The observed stress field in eastern North America is characterized by an ENE-WSW compression (Figure 10a). The directions of *SH*max within the plate interior are aligned along the orientation of small circles about the North America-Eurasia (na-eu) PoR, suggesting that the na-eu is an inward-displaced boundary. The transformed data show that the few data points adjacent to the plate boundary are scattered at various orientations. However, the stress field within the plate interior (at a distance of 25°-50°) is oriented along the predicted 90° azimuth with respect to the PoR (Figure 10c). The statistical tests also show a good agreement between the predicted and observed azimuths in this distance range (Figures 10f and 10h). The good fit to the data suggests that the stress field in eastern North America is dominated by buoyancy forces that arise from lateral density variations between mid-ocean ridges and plate interiors (ridge push), confirming *Richardson*'s [1992] results.

5.3.3. Western Europe. The observed direction of *SH*max in western Europe shows a distinct NW orientation (Figure 10b). Its alignment along small circles with respect to the Eurasia-Africa PoR suggests that the Eurasia-Africa is an inward-displaced boundary. The transformed data show a wide scatter of azimuths adjacent to the plate boundary, but a concentration of data around the predicted 90° at a distance of 20°-34° from the boundary (Figure 10d). The statistical tests also show a good agreement between the pre-

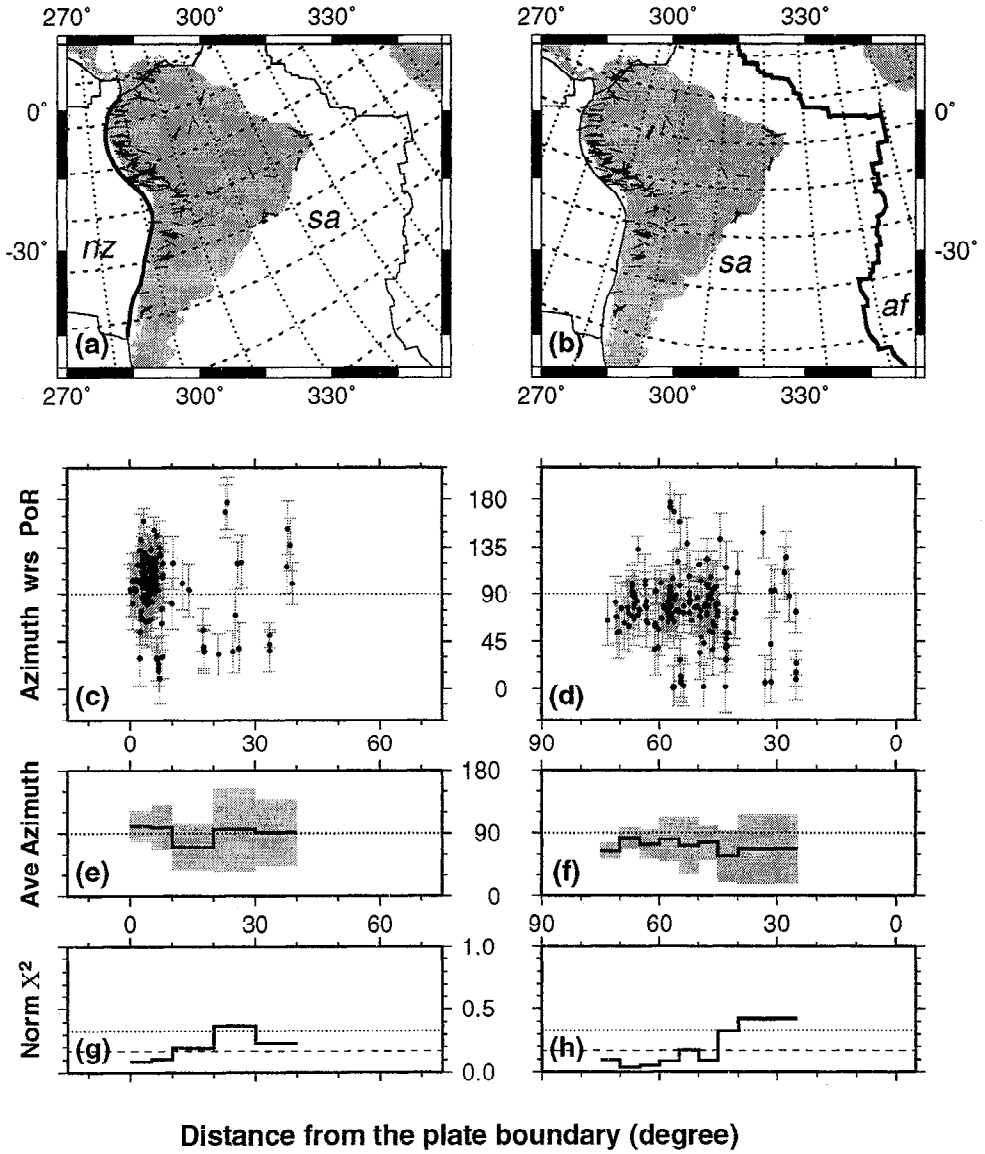

Figure 11. Intraplate stress field in South America adjacent to (a) the Nazca plate boundary and (b) the African plate boundary. The data, in both cases, are consistent with the predicted stress field for an inward-displaced boundary. See Figure 9 for details.

dicted and observed azimuths in this distance range, but not near to the plate boundary (Figures 10f and 10h) mainly due to the complex shape to the plate boundary along Italy and the Aegean. A slightly better fit of the near boundary average azimuth is obtained when the Hellenic arc is excluded from the plate boundary and the Adriatic Sea is included (dashed lines in Figures 10b, 10f, and 10h). A similar test conducted for the North America-Eurasia boundary showed 20°-30° misfit between the data and the orientation of small circles about the na-eu PoR. This misfit suggests that the stress field in western Eurasia is dominated by the collision forces acting along the Eurasia-Africa plate boundary. *Richardson* [1992] also attributed this stress field to collision forces; however, his calculations are based on torque calculations, in which their pole is located about 30° southwest of the NUVEL-1A na-eu PoR.

5.3.4. South America. The third set of tests compare the intraplate stress field in South America with the predictions of two possible inward-displaced plate boundaries: the South America-Nazca (sa-nz) and the South America-Africa (sa-af) (Figures 11a and 11b). The first test (sa-nz) analyzes the stress field as a result of deformation within a plate boundary region, whereas the second test (sa-af) analyzes the stress field as a plate interior region. Most of the observations are located along the western coast of South America (along the Andes) and show an E-W orientation of *SH*max , which aligns nicely along small circles around both poles of rotation. However, the stress data in eastern South America do not align with either pole, reflecting probably inhomogeneities within the ancient continental crust [*Zoback and Richardson*, 1996]. The transformed data with respect to both poles of rotation show a concen-

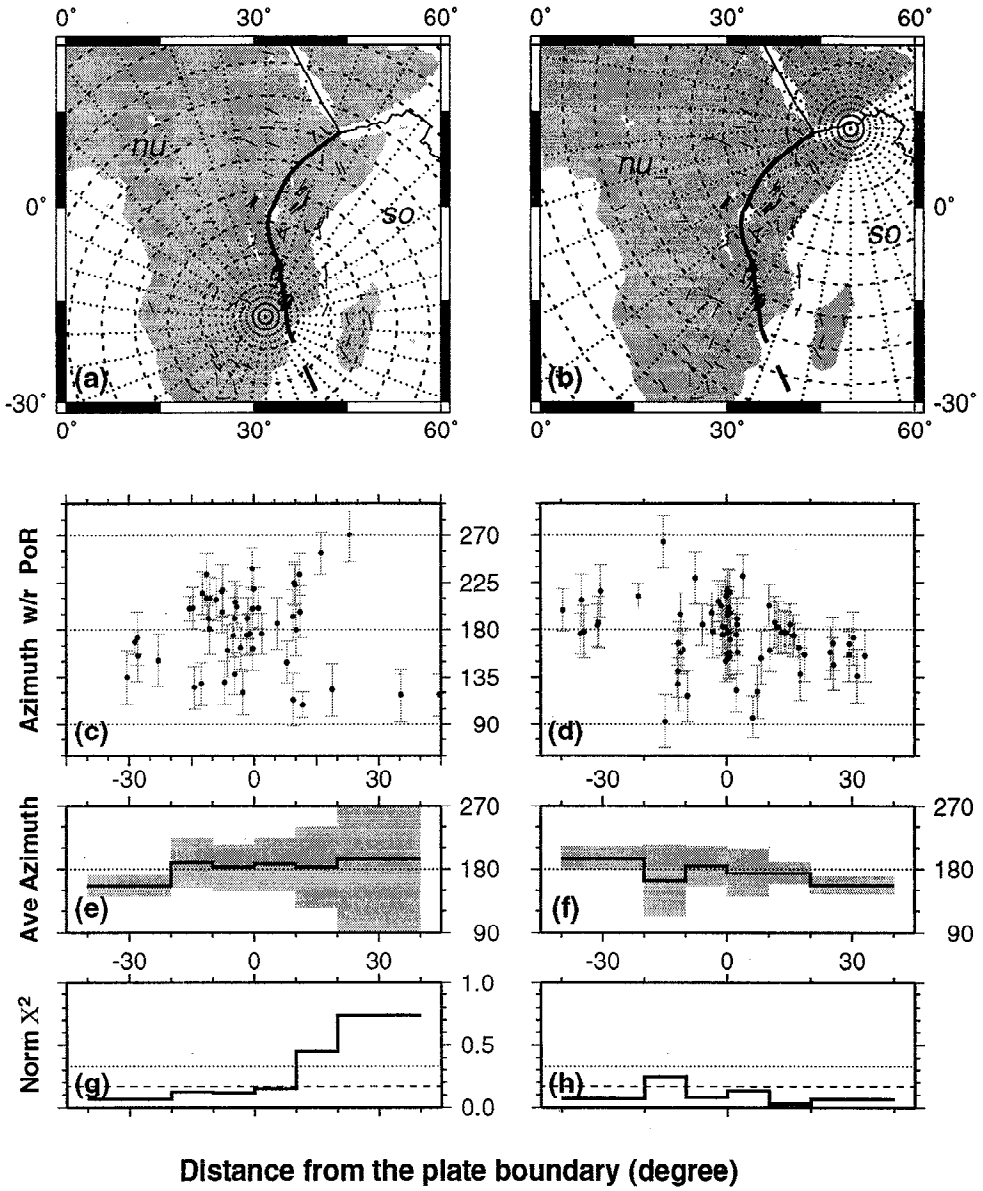

Figure 12. Intraplate stress field in East Africa adjacent to the Nubia-Somali plate boundary (a) according to *Wood et al.* [1985] Nubia-Somali PoR and (b) according to NUVEL-1A Australia-Africa PoR. See Figure 9 for details. The statistics of Figures 12e, 12f, 12g and 12h are operated on the range 90°-270° .

tration of the observed azimuths near the predicted 90° direction of an inward-displaced boundary (Figures 11c and 11d). The statistical tests show a good agreement between the predicted and observed azimuths at a distance of 0°-6° from the South America-Nazca plate boundary and at a distance of 35°-70° from the South America-Africa boundary. However, the overall fit (normalized χ^2 test) along the South America-Nazca plate boundary is better than that of South America-Africa boundary (Table 1), suggesting that the deformation along the Andes is dominated by collisional forces acting along the South America-Nazca plate boundary.

5.3.5. Eastern Africa. The stress field in eastern Africa is predominantly extensional. Its orientation (*SH*max) varies from E-W north of the equator, to NE-SW along the East African Rift (EAR), to N-S near the Indian Ocean coast (Figure 12). The active deformation along the EAR, including significant seismic activity (Figure 1), suggests that the EAR may be viewed as a deforming plate boundary region. Indeed, numerous studies have considered the EAR as a plate boundary separating Nubia from Somali and calculated the relative plate motion between the two plates [e.g., *Chase*, 1978; *Woods et al.*, 1985; *Joffe and Garfunkel*, 1987; *Jestin et al.*, 1994]. According to the theory, this is an outward-displaced boundary at which the direction of *SH*max should follow the orientation of great circles about the PoR (Figure 7). The major prob-

lem of testing this hypothesis is the unreliable determination of the PoR between the two plates. The only global plate motion model that includes the EAR as a plate boundary is P071 [*Chase*, 1978], which locates the pole in (71.4°S, 144.6°W). The more recent and reliable NUVEL-1A model does not separate Africa into two plates and therefore does not calculate the location of the Nubia-Somali PoR. However, *Woods et al.* [1985] and *Jestin et al.* [1994] used the NUVEL-1 data set to determine the pole at (17.5°S, 31.9°E) and (38.4°S, 8.7°E), respectively. A regional plate kinematic analysis of the circum Red Sea yielded a similar location of the PoR at (6.9°S, 33.0°E) [*Joffe and Garfunkel*, 1987]. I tested all four poles and found that the pole calculated by *Woods et al.* [1985] yields a predicted stress field that is consistent with the stress observations along the EAR (Figures 12a, 12c, 12e, and 12g); the width of the plate boundary according to this test is 10°-20°. The other three poles yield a stress field that is significantly less consistent with the observations. The overall pattern of the observed stress indicators in eastern Africa show a radial shape centered at the Gulf of Aden. This radial pattern is shown very clearly at the interpolated principal stress directions calculated by *Bird and Li* [1996, Figure 4] using nonparametric statistics. Coincidentally or not, the Gulf of Aden is also the location of the NUVEL-1A Australia-Africa PoR. I used this pole to test the stress field in eastern Africa (Figure 12b). As expected, this pole yielded a stress field that is more consistent with the observations (Figures 12d, 12f, and 12h). Furthermore, the predicted stress field according to this pole is consistent with the observation of a wide region (60°) around the EAR. This pole may represent the pole of the current deformation in eastern Africa.

6. Discussion

The proposed theory of intraplate tectonics uses simple assumptions about the mechanical behavior of deformable tectonic plates allowing it to link the well-established directions of relative plate motion to the direction of intraplate displacement and deformation fields in various tectonic environments. The theory's predictions are systematically compared with more than 4000 reliable stress indicators provided by the world stress map project [*Zoback*, 1992]. These comparisons show a good agreement between the predicted and observed directions of SHmax adjacent to the three types of deformable plate boundaries. Furthermore, best fit adjustment calculations (minimization of the normalized χ^2 tests) provide independent estimates for the width of the deforming regions (Table 1). According to the theory, intraplate deformation is induced by horizontal forces acting on plate lateral boundaries and by buoyancy forces that arise from lateral density variations between mid-ocean ridges and plate interiors (ridge push). These forces explain the primary compressive deformation observed in plate interiors and hence confirm *Richardson's* [1992] results. In addition, these forces also explain the extensional stress field in eastern Africa, which heretofore was attributed to intraplate buoyancy forces that arise due to the high topography and possibly thickened crust underlying this region [*Zoback*, 1992]. In plate boundary regions the deformation is explained solely by horizontal forces acting on plates lateral boundaries in the direction of relative plate motion. This explanation is consistent with *Ward's* [1988] megashear zone explanation suggested for the geodetic observed interseismic displacement rates across the Pacific-North America plate boundary. Expanding *Ward's* [1988] terminology, interseismic deformation along convergent and nonridge divergent plate boundaries may be viewed as megapush and megapull deforming zones, respectively, in which a finite width plate boundary zone is pushed or pulled as two adjacent plates move with respect to one another.

The theory also provides simple predictions of the first-order interseismic displacement rates in plate boundary regions. It predicts a linear decay of the displacement rate with distance from the boundary (equations (10) and (11)). Due to advances in space geodetic methods, displacement rates across many plate boundaries are observed nowadays and hence can be used to test the theory. A systematic comparison between the observed and predicted displacement rates requires a thorough analysis of the observations and their error budget, which is beyond the scope of this paper. Instead, I present one semi-quantitative test of geodetically observed displacement rates across the northern Baja and southern California segment of the Pacific-North America plate boundary, as presented by *Bennett et al.*, [1996] (Figures 3 and 13). The observed displacement rates were derived from GPS data collected in northern Baja and southern California during the years 1986-1995. Figure 13a shows the following patterns: (1) the displacement rates are primarily directed parallel to the direction of the relative motion between the Pacific and the North America plates, (2) their direction is not very sensitive to the direction and orientation of the plate boundary, and (3) their magnitude increases westward with distance from stable North America. In order to use these observations to test the theory, I first transform the observations to the Pacific-North America PoR spherical coordinate system (Figure 13b). The transformed displacement rates enhance the general pattern described above but also show slight misalignment of the observed directions with the orientation of small circles, which are represented here as vertical lines. The actual test is conducted by plotting the colatitudinal component of the transformed displacement rates, which is normalized by NUVEL-1A predicted relative plate motion, as a function of distance from the PoR (Figure 13c). A visual examination of the normalized colatitudinal component shows an almost continuous transition between the North American and Pacific plate velocities. This transition is modeled by a

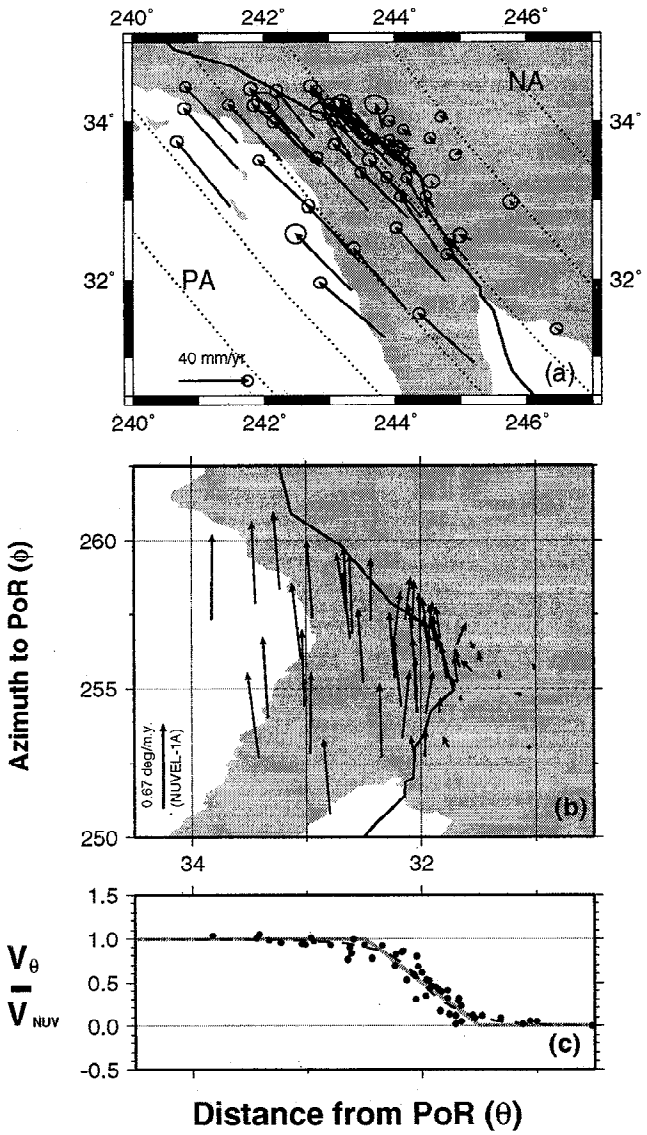

Figure 13. A test of the predicted interseismic displacement rate across the Pacific-North America plate boundary region. (a) Geodetically observed displacement rates (solid arrows) and the NUVEL-1A predicted relative plate motion (dotted lines) in Baja and southern California [after *Bennet et al.*, 1996] in a fixed North America reference frame. (b) Same observations transformed into the spherical coordinate system of the Pacific-North America PoR. (c) Displacement rate variations across the plate boundary. The colatitudinal component of the transformed displacement rates is normalized by the NUVEL-1A velocity. The transition from the stable North America plate velocity to the Pacific plate velocity occurs over a distance of 1°. It is modeled as linear transition (gray solid line) and by an exponential transition (dashed line).

straight line (solid gray line in Figure 13c) and by an exponential decay from a median value (dashed line in Figure 13c). Both models indicate that the width of the plate boundary is about 1 colatitudinal degree.

A similar analysis of geodetic data was conducted by *Ward* [1988], who analyzed VLBI data from North America according to a linear combination of the North America and Pacific velocities. His analysis is based on data from both northern and southern California and yield a much wider zone of deformation of 450 km, which is about 4°. I tested the same VLBI data using the more updated NUVEL-1A PoR between the two plates and derived a narrower width of the boundary, about 3°. The two data sets indicate width variations of the deforming plate boundary, in which the northern Baja and southern California segment is significantly narrower. The width of the entire boundary according to the stress data (Figure 9b and Table 1) extends over a much wider region (11°-13°). This width difference may represent strength variations within the deforming region, to which geodetic data are more sensitive than the orientation of SHmax . Another indication of strength variation across this diffuse plate boundary region is derived from the stress field contiguous to the San Andreas Fault, which is aligned perpendicular to the fault. The fault normal stress pattern is attributed to the very low strength of the fault, which cannot sustain significant shear stresses [*Zoback*, 1991]. Because the fault cannot transmit the shear stresses across the boundary, the overall 135° orientation of the far-field stress field (Figures 9b and 9d) is kept, most likely, due to basal tractions, which are not considered by the theory. However, the interseismic displacement rate and incremental strain rate fields do behave, to a first order, as predicted by the theory, suggesting that the incremental low magnitude shear stress is transmitted across the fault.

The width of the deforming region (D), which is determined using a best fit criterion, lies in the range of 4°-60° (Table 1). In most tested examples, the deforming region lies adjacent to the plate boundary. However, in eastern North America, eastern South America, western Europe, and India the best fitted deforming regions lie well within the plate interior (Table 1 and Figures 10 and 11). The location of the deforming region within the continental sections of eastern North America and eastern South America can be attributed to strength heterogeneities between strong oceanic and weaker nonstable continental lithospheres (assumption 3; Figure 6c). Although, localized inhomogeneities within the continental crust and the passive margins may also limit the extent of the deforming region [*Zoback and Richardson*, 1996]. The location of the deforming regions in western Europe and India, which lie more than 10° from the plate boundaries, reflects probably unmodeled effects, such as the complexity of the plate boundary geometry and intraplate buoyancy forces. However, the good fit of the data within the plate interior may indicate that in some continental regions the plate boundary forces are transmitted to the plate interior via the upper mantle rather than through the whole lithosphere.

The stress-determined estimate for the width of plate boundaries differs from geodetic, seismic, or structural

estimates of the width. As described above, the stress-determined width in southern California overestimates the geodetic-determined width. However, along the Aleutian arc (Figure 9a) the stress-determined width (4°) underestimates the actual width of the deforming region. Other indications of a misfit by the theory are determined from the poor χ^2 fitting, either within plate interiors, such as in Tibet (Table 1) or along plate boundaries, such as in southern Europe (Figure 10h). The poor fitting in Tibet probably reflects the neglect of intraplate buoyancy forces, which are the dominant driving force in that region, whereas the poor fitting in southern Europe probably reflects the complex plate boundary geometry not considered by the theory. The width differences and the poor χ^2 fitting points out the limitation of the theory, which is based on simple assumptions; the theory neglects the contribution of basal tractions, intraplate buoyancy forces, strength inhomogeneities, width variations along plate boundaries, and the geometry of plate boundaries. A more thorough analysis of the data will require a more careful testing of the data along smaller segments of plate boundaries and by modifying the theory to consider basal tractions and intraplate buoyancy forces.

The theory assumes elastic-plastic behavior of plates. Elastic deformation occurs at the interseismic stage of the earthquake deformation cycle and directed along the direction of relative plate motion. Plastic (permanent) deformation occurs along the weakest elements, which are usually existing fault planes, as the stress level exceeds the yield stress. Thus although the interseismic deformation is homogeneously distributed within the entire plate boundary regions, the permanent coseismic deformation is inhomogeneous and accumulates along faults. As a result, the short-term interseismic strain field does not necessarily coincide with the long-term accumulated strain in plate boundary regions. As long as the relative plate motion is normal or tangential to the boundary, the two strain fields will be oriented similar to one another. However, along obliquely converging (or extending) plate boundaries the short- and long-term strain fields may vary significantly from one another. In this tectonic environment, the long-term strain tends to partition between subduction normal to the plate boundary and strike-slip motion parallel to the boundary [*Fitch*, 1972]. The best example of such strain partitioning is observed along the Sumatra segment of the Australia-Eurasia plate boundary. At the interseismic stage, however, the theory predicts that elastic displacement and strain are oriented along the direction of relative plate motion, independent of the plate geometry. Hence the theory predicts that along the oblique convergence of Sumatra, the interseismic displacements and strain will follow the direction of plate motion at about 45° to the plate boundary geometry. Indeed, recent geodetic observations from Sumatra show that the interseismic displacement rates are predominantly oriented along the direction of relative plate motion and not parallel or normal to the boundary [*Prawirodirdjo et al.*, 1997].

7. Conclusions

The theory of intraplate tectonics, which expands upon the classical theory of plate tectonics, presents a new reference frame to evaluate and interpret intraplate deformation. It provides the theoretically expected first-order intraplate displacement, displacement rate, strain, and stress fields adjacent to three types of deformable plate boundaries: inward-, outward-, and tangential-displaced boundaries. By using spherical geometry, as in the theory of plate tectonics, the new theory yields simple predictions in terms of small circles, great circles, and 45° loxodromes around the PoR of two adjacent plates. The predicted stress field was systematically compared with more than 4000 reliable observations of the world stress map [*Zoback*, 1992] and found to be in good agreement with the observed stress field. The predicted displacement rate field was semi-qualitative compared with geodetically observed displacement rates across the northern Baja and southern California segment of the Pacific-North America plate boundary. A more rigorous comparison between the predicted and observed displacement field should be conducted in the near future, as more geodetic observations will be available. The simple predictions and their good agreement with the observations suggest that intraplate deformation should be investigated in the PoR spherical coordinate system.

The theory explains the observed first-order intraplate stress field as a result of horizontal forces induced by the neighboring plates in the direction of relative plate motion between two adjacent plates and by buoyancy forces that arise from lateral density variations between mid-ocean ridges and plate interiors (ridge push). It uses the same tectonic framework to explain the observed compressional, transcurrent, and extensional stress fields in the various tectonic environments. Thus it explains the observed first-order stress in western North America and Africa by horizontal forces acting on plate boundaries, and not by buoyancy forces, as suggested before.

Appendix: Transformations in Spherical Coordinates

This study uses spherical coordinate transformations to move from the pole of rotation (PoR) coordinate system to the geographic (north pole) system and vice versa. Both transformations use the fundamental rotation matrices, which are

$$\mathbf{R}_1 = \begin{pmatrix} 1 & 0 & 0 \\ 0 & \cos\omega_1 & -\sin\omega_1 \\ 0 & \sin\omega_1 & \cos\omega_1 \end{pmatrix} \quad \text{(A1a)}$$

$$\mathbf{R}_2 = \begin{pmatrix} \cos\omega_2 & 0 & \sin\omega_2 \\ 0 & 1 & 0 \\ -\sin\omega_2 & 0 & \cos\omega_2 \end{pmatrix} \quad \text{(A1b)}$$

$$\mathbf{R}_3 = \begin{pmatrix} \cos\omega_3 & -\sin\omega_3 & 0 \\ \sin\omega_3 & \cos\omega_3 & 0 \\ 0 & 0 & 1 \end{pmatrix} \quad \text{(A1c)}$$

The first transformation, from the PoR system to the geographic system, is used to calculate and plot the geographic coordinates of small and great circles and 45° loxodromes. This transformation requires the geographic location of the PoR (θ_P,ϕ_P) and a point Q' ($\theta_{Q'}$,$\phi_{Q'}$) in the PoR system. The transformation is

$$\mathbf{r} = \mathbf{R_3}(180^o - \phi_P)\ \mathbf{R_2}(90^o - \theta_P)\ (\mathbf{r}') \quad \text{(A2)}$$

where $\mathbf{r}$ is the transformed vector and $\mathbf{r}'$ is the Cartesian unit vector from the origin to the point Q' ($\mathbf{r}' = (\cos\theta_{Q'}\cos\phi_{Q'}\ ,\cos\theta_{Q'}\ \sin\phi_{Q'}\ ,\sin\theta_{Q'})$). The transformed colatitude and azimuth, in the geographic coordinate system, are

$$\theta_Q = -\tan^{-1}\left(\frac{r_1}{r_2}\right) \quad \text{(A3a)}$$

$$\phi_Q = 90^o - \sin^{-1}(r_3) \quad \text{(A3b)}$$

The second transformation, from the geographic system to the PoR system is used to test the success of the theory by comparing the predicted and observed directions of *SH*max in the PoR coordinate system. This transformation requires the geographic location of the PoR (θ_P,ϕ_P) and a point Q (θ_Q,ϕ_Q). The transformation is

$$\mathbf{r}' = \mathbf{R_2}(90^o - \theta_P)\ \mathbf{R_3}(180^o - \phi_P)\ (\mathbf{r}) \quad \text{(A2)}$$

where $\mathbf{r}$ is the Cartesian unit vector from the origin to the point Q in the geographic coordinate system and $\mathbf{r}'$ is the transformed vector. The transformed colatitude and azimuth, in the PoR coordinate system, are

$$\theta_{Q'} = -\tan^{-1}\left(\frac{r'_1}{r'_2}\right) \quad \text{(A3a)}$$

$$\phi_{Q'} = 90^o - \sin^{-1}(r'_3) \quad \text{(A3b)}$$

Acknowledgments. I am thankful to Randy Richardson, to the Associate Editor, Mike Ellis, and to an anonymous referee for their thorough review of the manuscript. I would also like to thank Amotz Agnon, Gary Axen, Yehuda Bock, Itai Hareven, Ditza Kempler, Robert Porth, Ross Stein, Celal Sengor, Joann Stock, and Jilles Wust for useful discussions and comments. I thank Randy Richardson and David Coblentz for supplying me with the needed data sets. The maps and figures were generated using the Generic Mapping tools (GMT) software [*Wessel and Smith*, 1991].

References

Argus, D.F., and R.G. Gordon, Pacific-North American plate motion from very long baseline interferometry compared with motion inferred from magnetic anomalies, transform faults, and earthquake slip vectors, *J. Geophys. Res., 95*, 17,315-17,324, 1990.

Argus, D.F., and R.G. Gordon, Tests of the rigid-plate hypothesis and bounds on intraplate deformation using geodetic data from very long baseline interferometry, *J. Geophys. Res., 101*, 13,555-13,572, 1996.

Argus, D.F., and M.B. Heflin, Plate motion and crustal deformation estimated with geodetic data from the Global Positioning System, *Geophys. Res. Lett., 22*, 1973-1976, 1995.

Bennett, R.A., W. Rodi, and R.E. Reilinger, Global Positioning System constraints on fault slip rates in Southern California and northern Baja, Mexico, *J. Geophys. Res., 101*, 21,943-21,960, 1996.

Bird, P., and J. Baumgardner, Fault friction, regional stress, and crust-mantle coupling in southern California from finite element models, *J. Geophys. Res., 89*, 1932-1944, 1984.

Bird, P., and J. Li, Interpolation of principal stress directions by nonparametric statistics: Global maps with confidence limits, *J. Geophys. Res., 101*, 5435-5443, 1996.

Chase, C.G., Plate kinematics: The Americas, East Africa, and the rest of the world, *Earth Planet. Sci. Lett., 37*, 355-368, 1978.

Chinnery, M.A., The deformation of the ground around surface faults, *Bull. Seismol. Soc. Am., 51*, 355-372, 1961.

Chinnery, M.A., The stress changes that accompany strike-slip faulting, *Bull. Seismol. Soc. Am., 53*, 921-932, 1963.

Cloetingh, S.A.P.L., and M.J.R. Wortel, Regional stress field of the Indian plate, *Geophys. Res. Lett., 12*, 77-80, 1985.

Cloetingh, S.A.P.L., and M.J.R. Wortel, Stress in the Indo-Australian plate, *Tectonophysics, 132*, 49-67, 1986.

Coblentz, D.D., and R.M. Richardson, Statistical trends in the intraplate stress field, *J. Geophys. Res., 100*, 20,245-20,256, 1995.

Coblentz, D.D., and R.M. Richardson, Analysis of the South America intraplate stress field, *J. Geophys. Res., 101*, 8643-8657, 1996.

DeMets, C., R.G. Gordon, D.F. Argus, and S. Stein, Effect of recent revisions to the geomagnetic reversal time scale on estimates of current plate motions, *Geophys. Res. Lett., 21*, 2191-2194, 1994.

Dixon, T.H., GPS measurements of relative motion of the Cocos and Caribbean plates and strain accumulation across the middle America trench, *Geophys. Res. Lett., 20*, 2167-2170, 1993.

Ekstrom, G., and P.C. England, Seismic strain rates in regions of distributed continental deformation, *J. Geophys. Res., 94*, 10,231-10,257, 1989.

England, P.C., and D.P. McKenzie, A thin viscous sheet model for continental deformation, *Geophys. J. R. Astron. Soc., 70*, 295-321, 1982.

Feigl, K.L., et al., Space geodetic measurement of crustal deformation in central and southern California, 1984-1992, *J. Geophys. Res., 98*, 21,677-21,712, 1993.

Fitch, T.J., Plate convergence, transcurrent faults and internal deformation adjacent to southeast Asia and the western Pacific, *J. Geophys. Res., 77*, 4432-4460, 1972.

Forsyth, D.W., and S. Uyeda, On the relative importance of the driving forces of plate motion, *Geophys. J. R. Astron. Soc., 43*, 163-200, 1975.

Fung, Y.C., *Foundations of Solid Mechanics*, Prentice-Hall, Englewood Cliffs, N. J., 1968.

Gordon, R.G., Plate motion, crustal and lithospheric mobility, and paleomagnetism: Prospective viewpoint, *J. Geophys. Res., 100*, 24,367-24,392, 1995.

Gough, D.I., Mantle flow under North America and plate dynamics, *Nature, 311*, 428-433, 1984.

Haines, A.J., Calculating velocity field across plate bound-

aries from observed shear rates, *Geophys. J. R. Astron. Soc., 68*, 203-209, 1982.

Haines, A.J., and W.E. Holt, A procedure for obtaining the complete horizontal motions within zone of distributed deformation from the inversion of strain rate data, *J. Geophys. Res., 98*, 12,057-12,082, 1993.

Herring, T.A., et al., Geodesy by radio interferometry: Evidence for contemporary plate motion, *J. Geophys. Res., 91*, 8341-8347, 1986.

Isacks, B., J. Oliver, and L. R. Sykes, Seismology and the new global tectonics, *J. Geophys. Res., 73*, 5855-5899, 1968.

Jackson, J.A., and D.P. McKenzie, Active tectonics of the Alpine-Himalaya belt between western Turkey and Pakistan, *Geophys. J. R. Astron. Soc., 77*, 185-264, 1984.

Jackson, J.A., and D.P. McKenzie, The relationship between plate motions and seismic moment tensors, and the rate of active deformation in the Mediterranean and the Middle East, *Geophys. J. R. Astron. Soc., 93*, 45-73, 1988.

Jestin, F., P. Huchon, and J.M. Gaulier, The Somalia plate and the East African Rift System: Present-day kinematics, *Geophys. J. Int., 116*, 637-654, 1994.

Joffe, S., and Z. Garfunkel, Plate kinematics of the circum Red Sea: A re-evaluation, *Tectonophysics, 141*, 5-22, 1987.

Kanamori, H., The state of stress in the Earth's lithosphere, in *Physics of the Earth's Interior*, edited by A.M. Dziewonski and E. Boschi, pp. 531-552, North-Holland, New York, 1980.

Li, V.C., and J.R. Rice, Crustal deformation in great California earthquake cycles, *J. Geophys. Res., 92*, 11,533-11,551, 1987.

Ma, C., J.W. Ryan, and D.S. Caprette, Crustal Dynamics Project data analysis, VLBI geodetic results 1979-1990, *NASA Tech. Memo. 104552*, 1992.

Matsu'ura, M., D.D. Jackson, and A. Cheng, Dislocation model for the aseismic crustal deformation at Hollister, California, *J. Geophys. Res., 91*, 12,661-12,674, 1986.

Meijer, P.T., and M.J.R. Wortel, The dynamics of motion of the South American plate, *J. Geophys. Res., 97*, 11,915-11,931, 1992.

Molnar, P., Continental tectonics in the aftermath of plate tectonics, *Nature, 335*, 131-137, 1988.

Morgan, W.J., Rises, trenches, great faults, and crustal blocks, *J. Geophys. Res., 73*, 1959-1982, 1968.

Prawirodirdjo, L., et al., Geodetic observations of interseismic strain segmentation at the Sumatra subduction zone, *Geophys. Res. Lett., 24*, 2601-2604, 1997.

Ranalli, G. *Rheology of the Earth, Deformation and Flow Processes in Geophysics and Geodynamics*, pp. 1-365, Allen and Unwin, Winchester, Mass., 1987.

Ray, J.R., C. Ma, J.W. Ryan, T.A. Clark, R.J. Eanes, M.M. Watkins, B.E. Schutz, and B.D. Tapley, Comparison of VLBI and SLR geocentric site coordinates, *Geophys. Res. Lett., 18*, 231-234, 1991.

Richardson, R.M., Ridge forces, absolute plate motions, and the intraplate stress field, *J. Geophys. Res., 97*, 11,739-11,748, 1992.

Richardson, R.M., and L.M. Reding, North American plate dynamics, *J. Geophys. Res., 96*, 12,201-12,223, 1991.

Richardson, R.M., S.C. Solomon, and N.H. Sleep, Tectonic stress in the plates, *Rev. Geophys., 17*, 981-1019, 1979.

Savage, J.C., A dislocation model of strain accumulation and release at a subduction zone, *J. Geophys. Res., 88*, 4984-4996, 1983.

Savage, J.C., Equivalent strike-slip earthquake cycles in half-space and lithosphere-asthenosphere Earth models, *J. Geophys. Res., 95*, 4873-4879, 1990.

Sbar, M.L., and L.R. Sykes, Contemporary compressive stress and seismicity in eastern North America: An example of intraplate tectonics, *Geol. Soc. Am. Bull., 84*, 1861-1882, 1973.

Smith, D.E., R. Kolenkiewicz, P.J. Dunn, J.W. Robbins, M.H. Torrence, S.M. Klosko, R.G. Williamson, E.C. Pavli, N.B. Douglas, and S.K. Fricke, Tectonic motion and deformation from Satellite Laser Ranging to LAGEOS, *J. Geophys. Res., 95*, 22,013-22,041, 1990.

Stefanick, M., and D.M. Jurdy, Stress observations and driving force models for the South American plate, *J. Geophys. Res., 97*, 11,905-11,913, 1992.

Tapponnier, P., and P. Molnar, Slip-line field theory and large-scale continental tectonics, *Nature, 264*, 319-324, 1976.

Tregoning, P., F.K. Brunner, Y. Bock, E. Calais, J.F. Genrich, S.S.O. Puntodewo, C. Subarya, J. Rais, and R. McCaffrey, First geodetic measurement of convergence across the Java trench, *Geophys. Res. Lett., 21*, 2135-2138, 1994.

Turcotte, D.L., and G. Schubert, *Geodynamics, Application of Continuum Physics to Geological Problems*, pp. 1-450, John Wiley, New York, 1982.

Vilotte, J.P., M. Daigniére, and R. Madariaga, Numerical modeling of intraplate deformation: simple mechanical models of continental collision, *J. Geophys. Res., 87*, 10,709-10,728, 1982.

Ward, S.N., North America-Pacific plate boundary, an elastic-plastic megashear: Evidence from very long baseline interferometry, *J. Geophys. Res., 93*, 7716-7728, 1988.

Wdowinski, S., and Y. Bock, The evolution of deformation and topography of high elevated plateaus, 1, Model, numerical analysis, and general results, *J. Geophys. Res., 99*, 7103-7119, 1994.

Wdowinski, S., R.J. O'Connell, and P. England, Continuum models of continental deformation above subduction zones: Application to the Andes and the Aegean, *J. Geophys. Res., 94*, 10,331-10,346, 1989.

Wempner, G., *Mechanics of Solids With Applications to Thin Bodies*, McGraw-Hill, New York, 1973.

Wessel, P., and W.H.F. Smith, Free software helps map and display data, *Eos Trans. AGU, 7272 (41)*, 441, 445-446, 1991.

Woods, D.F., et al., Constraints on Nubia-Somalia rifting from NUVEL-1 relative plate motion data (abstract), *Eos Trans. AGU, 66*, 1062, 1985.

Yang, J.-P., and Y.P. Aggarwal, Seismotectonics of northeastern United States and adjacents Canada, *J. Geophys. Res., 86*, 4981-4998, 1981.

Zoback, M.D., State of stress and crustal deformation along weak transform faults, *Philos. Trans. R. Soc. London Ser. A, 337*, 141-150, 1991.

Zoback, M.D., and M.L. Zoback, State of stress and intraplate earthquakes in the central and eastern United States, *Science, 213*, 96-104, 1981.

Zoback, M.L., First- and second-order patterns of stress in the lithosphere: The world stress map project, *J. Geophys. Res., 97*, 11,703-11,728, 1992.

Zoback, M.L., and R.M. Richardson, Stress perturbation associated with the Amazonas and other ancient continental rifts, *J. Geophys. Res., 101*, 5459-5475, 1996.

Zoback, M.L., and M.D. Zoback, State of stress of the conterminous United States, *J. Geophys. Res., 85*, 6113-6156, 1980.

Zoback, M.L., et al., Global patterns of tectonic stress, *Nature, 341*, 291-298, 1989.

S. Wdowinski, Department of Geophysics and Planetary Sciences, Tel Aviv University, Ramat Aviv 69978, Israel. (e-mail: shimon@geo1.tau.ac.il)

(Received July 9, 1996; revised November 7, 1997; accepted November 14, 1997.)